Thesis for the Degree of Doctor of Philosophy

Air-gap spinning of lignin-cellulose fibers

Jenny Bengtsson

CHALMERS

Department of Chemistry and Chemical Engineering
Chalmers University of Technology
Göteborg, Sweden 2021

Air-gap spinning of lignin-cellulose fibers

JENNY BENGTSSON
ISBN 978-91-7905-491-5

Doktorsavhandlingar vid Chalmers tekniska högskola
Ny serie nr 4958
ISSN 0346-718X

Chalmers University of Technology
Department of Chemistry and Chemical Engineering
SE-412 96 Göteborg, Sweden
Phone: +46 (0)31-772 10 00

Cover:
A tiny knot of a lignin-cellulose fiber,
captured with a scanning electron microscopy.

Printed by Chalmers Reproservice
Göteborg, Sweden 2021

Air-gap spinning of lignin-cellulose fibers

Jenny Bengtsson

Department of Chemistry and Chemical Engineering
Chalmers University of Technology

Abstract

Co-processing of lignin and cellulose, the two main constituents of wood, has previously been identified as a potential route for the production of inexpensive and bio-based carbon fibers. The first step in this process is to spin a precursor fiber. This can be done with different techniques, and the specific characteristics of air-gap spinning of solutions containing lignin and cellulose were investigated in this work. Studies on how the addition of lignin to a cellulose solution affect the spinnability, the coagulation process, and the fiber structure and properties were performed.

In accordance with the hypothesis, it was found that it was possible to gain advantages from both materials, by combining cellulose and lignin. Cellulose is a stiff and linear polymer that contributed to the strength of the fiber, while lignin, with its high carbon content, enhanced the final yield after conversion into carbon fiber.

Additionally, solutions that contained both lignin and cellulose could be air-gap spun at substantially higher draw ratios than pure cellulose solutions. This improvement could not be explained with the shear rheology results, however, based on measurements of the take-up force during spinning it was proposed that lignin stabilize against diameter fluctuations during spinning. To analyze how lignin affects the coagulation of lignin-cellulose fibers the total mass transport during coagulation was studied. Different coagulation baths were used, and it was found that minor parts of the lignin leached out, the amount correlated to the lignin solubility in the coagulation bath. Nevertheless, from the results it could also be concluded that the addition of lignin to a cellulose solution did not hinder the coagulation of the fibers. Regarding the fiber structure, it was possible to analyze the molecular order of cellulose and lignin separately and the lignin was found to be completely disordered also in a stretched fiber. In contrast, cellulose attained a preferred molecular orientation even in fibers with high lignin ratios. To further assess the full potential of the system, the lignin-cellulose fibers that were produced were also converted into carbon fibers, and the mechanical properties are promising. In summary, it was considered that lignin-cellulose based carbon fibers have great potential in becoming commercially available if efforts are continued in increasing the strength and stiffness of the fibers even further together with the implementation of efficient solvent recycling.

Keywords: *lignin, cellulose, ionic liquid, air-gap spinning, carbon fibers*

List of Publications

Paper I **Improved yield of carbon fibers from cellulose and kraft lignin**
Andreas Bengtsson, Jenny Bengtsson, Carina Olsson, Maria Sedin, Kerstin Jedvert, Hans Theliander and Elisabeth Sjöholm
Holzforschung, **2018**, 72, 1007-1016.

Paper II **Mass transport and yield during spinning of lignin-cellulose carbon fiber precursors**
Jenny Bengtsson, Kerstin Jedvert, Artur Hedlund, Tobias Köhnke and Hans Theliander
Holzforschung, **2019**, 73 (5), 509-516.

Paper III **Identifying breach mechanism during air-gap spinning of lignin-cellulose ionic-liquid solutions**
Jenny Bengtsson, Kerstin Jedvert, Tobias Köhnke and Hans Theliander
Journal of Applied Polymer Science, **2019**, 36(30), 47800.

Paper IV **Disassociated molecular orientation distributions of a cellulose–lignin carbon fiber precursor: A study by rotor synchronized NMR spectroscopy and X-ray scattering**
Leo Svenningsson, Jenny Bengtsson, Kerstin Jedvert, Werner Schlemmer, Hans Theliander and Lars Evenäs
Carbohydrate Polymers, **2021**, 254, 117293 .

Paper V **The challenge of predicting spinnability: investigating benefits of adding lignin to cellulose solutions in air-gap spinning**
Jenny Bengtsson, Kerstin Jedvert, Tobias Köhnke and Hans Theliander
Journal of Applied Polymer Science, **2021**, 138 (26), 50629.

Contribution report

The author's contribution to the papers presented in this thesis:

Paper I	Partly responsible for the experimental outline. Conducted all experimental work regarding production and characterization of lignin-cellulose fibers. Contributed to evaluating results and preparing the manuscript.
Paper II	Main author. Responsible for experimental outline, performing the experimental work, and interpreting the results.
Paper III	Main author. Responsible for experimental outline, method development, performing the experimental work, and interpreting the results.
Paper IV	Partly responsible for the experimental outline. Conducted experimental work regarding production and birefringence measurements of lignin-cellulose fibers. Contributed to evaluating results and preparing the manuscript.
Paper V	Main author. Responsible for experimental outline, method development, performing the experimental work, and interpreting the results.

Results related to this work have also been presented at the following conferences:

Coagulation of dry-jet wet-spun lignin-based carbon fibre precursors
Jenny Bengtsson, Kerstin Jedvert, Tobias Köhnke and Hans Theliander
15th European Workshop on Lignocellulosics and Pulp,
Aveiro, Portugal, June **2018**, pp. 123-126.
(Poster)

Dry-jet wet-spun lignin-based carbon fibre precursors: Phenomena and properties
Jenny Bengtsson, Kerstin Jedvert, Tobias Köhnke and Hans Theliander
255th National Meeting and Exposition of the American-Chemical-Society, ACS,
New Orleans, USA, March **2018**.
(Oral presentation)

LightFibre – Lignin-based carbon fibres from solution spun prefibres
Jenny Bengtsson, Tobias Köhnke, Hans Theliander and Carina Olsson
The Lignin Center of Sweden, 1st Workshop
Stockholm, Sweden, March **2017**, pp. 4.
(Oral presentation)

Additional publications, not included in thesis:

Carbon fibers from lignin-cellulose precursors: effect of stabilization conditions
Andreas Bengtsson, Jenny Bengtsson, Maria Sedin and Elisabeth Sjöholm
ACS Sustainable Chemistry and Engineering, **2019**, 7, 8440-8448.

Abbreviations

AGU	Anhydroglucose units
CF	Carbon fiber
CFRP	Carbon fiber reinforced plastics
COP	Cross-over point
DMSO	Dimethyl sulfoxide
EMIMAc	1-Ethyl-3-methylimidazolium acetate
GPC	Gel permeation chromatography
LAOS	Large amplitude oscillatory shear
MW	Molecular weight
MWD	Molecular weight distribution
NMMO	N-methyl morpholine N-oxide
NMR	Nuclear magnetic resonance
PAN	Polyacrylonitrile
RH	Relative humidity
RL5	Retentate lignin 5 kDa MW cut-off
RL15	Retentate lignin 15 kDa MW cut-off
ROSMAS	Rotor synchronized magic-angle spinning
SEM	Scanning electron microscopy
TM	Tensile modulus
TS	Tensile strength
UV	Ultraviolet

Contents

1 Introduction

Extruding solutions and shaping of polymers into continuous fibers have been done for over a hundred years. The first experiments with spinning of cellulose fibers were conducted in the late 19^{th} century (Woodings, 2001). However, after an initial increase, the production levels of man-made cellulose fibers remained fairly constant throughout the second half of the next century, as synthetic fibers absorbed the whole share of the annual market increase. At the beginning of the new millennium, regenerated cellulose fibers are again on the rise. This is mainly a result of difficulties in expanding global cotton production in combination with the ambition to replace of fossil-based polymers with fibers made from bio-based raw materials (The Fiber Year, 2019).

In order to meet the increasing demand for bio-based fibers, new raw materials are being considered both for textile and technical applications. Many bio-based raw materials, such as cellulose, do not melt. Instead, cellulose is degraded if heated at too high temperatures. Thus, suitable solvents are required to enable reshaping into fibers. The properties of the final fiber is often extensively studied when evaluating new raw materials. However, what may not be obvious, but of equal importance for the fiber production, is the need to also study spinning performance, as new raw materials may also alter the spinning process. Depending on what kind of – or what mixture of – polymers and solvents that are used, these changes can have a substantial impact on the properties of the spinning solution and, consequently, have a major influence on how easily the solution can be shaped into fibers. For this reason, it is essential to investigate overall spinning performance in order to evaluate the feasibility of fiber production when considering new raw materials for fiber applications. In this work, lignin and cellulose were mixed into solution and co-extruded into fibers, and the different steps of fiber production were elucidated.

The reason why lignin and cellulose should be spun together originates from the interest in inexpensive bio-based carbon fibers. Carbon fibers are made from polymeric precursor fibers that undergo several steps of thermal treatments. The current commercial carbon fibers are produced from expensive and fossil-based precursors (Baker & Rials, 2013). A less expensive carbon fiber, preferably with a lower car-

bon footprint, could be used as reinforcement in lightweight composites (carbon fiber reinforced plastics, CFRP) and used as structural elements in cars, for example. The total weight of a vehicle could be reduced if part of the steel was replaced with CFRP. This would contribute to a better fuel economy and less environmental impact (Souto *et al.*, 2018). Lignin has a high carbon content and has thus been considered as a relevant raw material for the production of carbon fibers for several decades (Baker & Rials, 2013). A carbon fiber made from lignin is considered a more sustainable alternative than the current commercial precursors (Hermansson *et al.*, 2019).

Lignin and cellulose from wood are available in large quantities in existing production in the pulping industry. Lignin, in particular, is currently an underutilized natural resource, as it is most often only used in energy recovery (Gellerstedt, 2015). However, as for now, no carbon fiber produced from pure lignin fibers has exhibited acceptable mechanical properties (Baker & Rials, 2013). Cellulose can, in contrast, be used to make strong carbon fibers, however, the yield in the carbon fiber production is low (Frank *et al.*, 2014). Using lignin and cellulose together in one fiber is based on the idea of combining the benefits of both lignin and cellulose: yield and strength (Olsson *et al.*, 2017; Garoff *et al.*, 2015). Fibers of lignin and cellulose can be created with air-gap spinning, which is a type of wet spinning. In this technique, lignin and cellulose are simultaneously dissolved in a solvent, extruded into fibers, and then precipitated in a coagulation bath (Lehmann *et al.*, 2012). The lignin-cellulose fibers can then be used as precursors in the subsequent conversion to carbon fibers The long-term goal of this route is to create an inexpensive carbon fiber with low environmental impact that can be used in a broader range of applications than current commercial carbon fibers.

1.1 Objectives

The main objective of this work was to investigate the air-gap spinning of lignin-cellulose fibers and to gain knowledge about how the addition of lignin to a cellulose solution affects different stages of the process. In a wider context, the results were used to evaluate the potential of lignin-cellulose fibers for use as carbon fiber precursors. The overall hypothesis was that by combining cellulose and lignin in one fiber, cellulose would enhance the strength of the fiber, while lignin, with its high carbon content, would increase the carbon fiber yield.

Studies on the extrusion, coagulation and final fiber structure were performed to assess the impact of lignin on the spinning process. New methods were developed to analyze the extrusion that enabled identification of the mechanisms that cause breakage during air-gap spinning. The raw materials were varied, and the lignin yield during coagulation and molecular structure of the spun fibres was evaluated.

2 Air-gap spinning of fibers

All spinning processes have in common that fibers are formed by a fluid being forced through a nozzle, in many cases a die with multiple capillaries, and the extruded fluid is thereafter solidified in its new shape, fibers. There are traditionally three main spinning processes: melt, wet, and dry spinning. In melt spinning the fluid is a polymer melt, and in both wet and dry spinning the fluid is a polymer solution. The distinction between wet and dry spinning lies in the fixation of the fiber: in wet spinning the fibers solidifies in a coagulation bath and in dry spinning, the solvent evaporates which causes the fibers to solidify (Gries *et al.*, 2015). Additionally, there is a modified type of wet spinning: dry-jet wet spinning, also known as air-gap spinning. This is the method used in the present work.

Air-gap spinning was initially developed for aramid fibers where the spinning dope and coagulation bath had to be at different temperatures, especially when the spinning solution was 90 °C or higher (Morgan, 1964; Mortimer & Peguy, 1996). In air-gap spinning, the extruded polymer solution is first let through air, or other gas, before entering a coagulation bath, see Figure 1 (Stibal *et al.*, 2005). One of the main advantages of air-gap spinning over wet spinning is that the air gap allows the solution to be stretched and, thus, create an alignment of the polymer chains before fiber fixation. Air-gap spinning can consequently be used to spin fibers with a high molecular orientation. To enable this spinning technique, it requires a polymer solution with a certain viscosity and elasticity, generally higher than solutions suitable for wet spinning. Nevertheless, the technique offers flexibility since the die and coagulation bath can be at different temperatures, and thus the polymer concentrations and solvents can be widely varied (Sixta *et al.*, 2015; Mortimer & Peguy, 1996). Neither wet spinning nor air-gap spinning can be performed as fast as melt spinning. Air-gap spinning is industrially performed in the order of 100 m/min, while melt spinning can achieve over 1000 m/min. There are two factors that limit the maximum operation speed: the fixation of the fibers proceeds slower, mass transport is less rapid than heat transfer (cooling), and the friction generated from pulling the fibers through the coagulation bath (Mortimer & Peguy, 1996; Gupta, 1997).

Both wet spinning and air-gap spinning are performed industrially to produce cel-

lulose fibers. Commercial cellulose fibers include, among others, viscose and lyocell. Viscose fibers are wet-spun, and the viscose process offers high flexibility. Fibers with very different properties can be produced, from textile-grade fibers to high-strength tire cords (Liebert, 2010). Lyocell fibers are air-gap spun and have, as a result of the spinning technique, greater mechanical strength than viscose fibers (Gries *et al.*, 2015).

The parameters in air-gap spinning that highly affect the fiber properties are, *e.g.* draw ratio and choice of coagulation liquid. Draw ratio is defined as the ratio between take-up velocity, v_t, and extrusion velocity, v_0, cf. Figure 1. The tenacity of cellulose fibers has been found to improve with draw ratio, up to approximately a draw ratio equal to 5-6, after this the tenacity reached a plateau value, *i.e.*, did not increase despite an increased draw ratio (Sixta *et al.*, 2015; Elsayed *et al.*, 2021). However, any draw ratio at which a tenacity plateau is reached for lignin-cellulose fibers has not yet been determined.

When the extruded fiber enters the coagulation bath, the coagulation liquid, a non-solvent, first causes the fiber to swell. The entered nonsolvent then solvates the cellulose solvent, which in turn starts to diffuse out of the fiber (Hedlund *et al.*, 2017). Coagulation proceeds at different speeds depending on the nonsolvent used. A higher affinity between nonsolvent and solvent contributes to faster coagulation. The choice of nonsolvent also affects the morphology of the fibers, such as porosity and crystallinity (Östlund *et al.*, 2013).

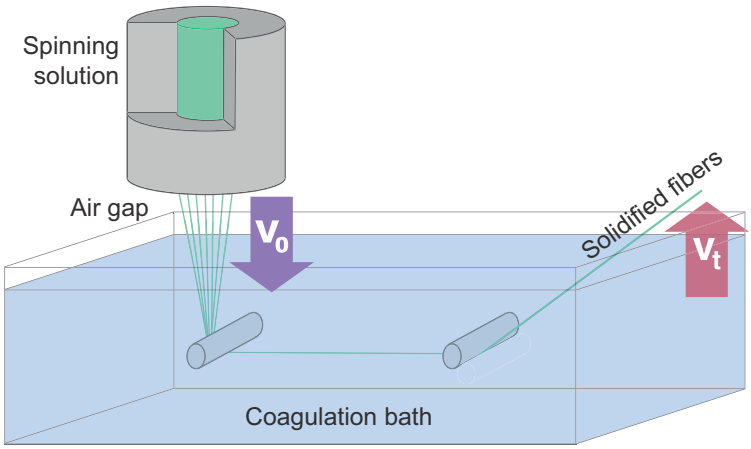

Figure 1. Overview of the air-gap spinning process

The fineness, T, of the spun fibers will be determined by the take-up velocity together with the polymer mass flow rate, M, according to Equation 1 (Stibal *et al.*, 2005). By expressing take-up velocity in terms of extrusion velocity and draw ratio, D_R, it is possible to see that the fineness only depends on the capillary size, R_0, polymer concentration in the solution, ρ^* expressed in $g\,polymer/m^3\,solution$ and draw ratio.

tex is a common unit for textile fibers and corresponds to g/1000 m.

$$T[tex] = \frac{M}{v_t} = \frac{\pi R_0^2 \rho^*}{D_R} \tag{1}$$

A closer look at the extrusion reveals another phenomenon during air-gap spinning that is also observed in melt spinning. When the solution exits the die, the stored elastic energy from shearing into the capillaries causes the solution to swell (Malkin & Isayev, 2017). This elastic recovery is called die swell. As a consequence of die swell, the velocity of the fiber is lower than the set extrusion velocity. The true draw ratio might, therefore, be higher than the measured draw ratio during spinning due to the lower velocity of the fiber after the die.

The solvent used in the process is chosen according to the fiber material, which was lignin and cellulose in the current work. The resulting properties of the spinning solution determine the stability of the overall process, *i.e.* the spinnability.

2.1 Solutions with lignin and cellulose

Lignin may be melted and used in melt spinning. However, cellulose will degrade instead of melting, and thus forming lignin-cellulose fibers requires a solvent in order to perform spinning. The following sections will describe the structure of lignin and cellulose, and discuss the available solvents.

2.1.1 Lignin

Lignin is found in the cell walls of wood and other plants, intermixed with cellulose and hemicelluloses. For example, softwood typically consists of around 40% cellulose and 26 % lignin. The biological function of lignin in plant cell walls is complex: lignin contributes to the rigidity of the plant, its water-impermeability, and acts as an anti-microbial agent. There are also strong indications that some of the lignin is covalently linked to the carbohydrates(Henriksson, 2017).

Native lignin is an amorphous polyphenolic, and there are three conventional, and predominant, monomers of lignin: p-coumaryl, coniferyl, and sinapyl alcohols, as shown in Figure 2. These are often referred to as hydroxyphenyl (H), guaiacyl (G), and syringyl (S) units respectively, depending on the structures formed in the polymer. There are most likely several other types of lignin monomers as well. The other types of monomers are mainly distinguished from conventional monomers by various acetyl groups linked to the γ-hydroxyl (Ralph *et al.*, 2004). The ratio of lignin monomers in different types of wood has been investigated, and the lignin in softwood consists mainly of guaiacyl units (>95%), while hardwood includes a mixture of essentially guaiacyl and synrigyl units (Gellerstedt & Henriksson, 2008)

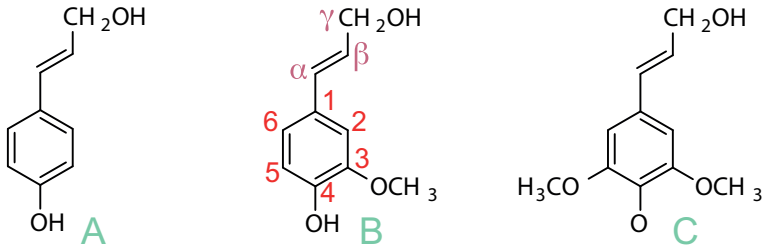

Figure 2. Predominant monomers of lignin (Gellerstedt & Henriksson, 2008). From the left: **A.** p-coumaryl alcohol (H), **B.** coniferyl alcohol (G), **C.** sinapyl alcohol (S). The conventional numbering (1-6 and $\alpha - \gamma$) of the carbon atoms in the lignin molecule is shown for the coniferyl alcohol.

Many investigations have characterized the different types of linkages in the lignin structure. The most prominent linkage in lignin structure is the ether bond β-O-4 (Gellerstedt & Henriksson, 2008), but several other ether and carbon-carbon linkages are also present (Ralph *et al.*, 2004). Isolated lignin, or technical lignins, discussed further in Section 2.1.3, may be melted, and the softening temperature is often around 150 °C (Gellerstedt, 2015).

2.1.2 Cellulose

Most often cellulose is incorporated in the cell walls of plants in a mixture of lignin and hemicelluloses, where the cellulose macrofibrils act as the reinforcement. This is the case in wood, and wood pulp is the dominant cellulose source for further processing (Klemm *et al.*, 2005). Cellulose belongs to the polysaccharides and consists of D-glucopyranose units, so-called anhydroglucose units (AGU), which are linked via β-glycosidic bonds. The three hydroxyl groups on each AGU are all in the equatorial position, and they form both inter- and intra-molecular hydrogen bonds, see the example in Figure 3. Cellulose chains are thus rigid, resulting from a combination of intra-molecular hydrogen bonds and the equatorial glycosidic linkage (Heinze *et al.*, 2012).

Cellulose forms crystalline structures. The equatorial inter-molecular hydrogen bonds arrange the cellulose chains in layers. The layers are then stacked on top of each other, held together by hydrophobic interactions. Depending on the rotational conformation of the C6-hydroxyl group, cf. Figure 3, the cellulose chains can form hydrogen bonds in various manners, and thereby giving rise to several different crystalline arrangements of cellulose. Native cellulose exists in the form of Cellulose I, composed of cellulose sheets with parallel chains. If cellulose is dissolved and then coagulated or regenerated, it will crystallize into Cellulose II, where the cellulose chains are arranged anti-parallel to each other, as this is a thermodynamically more stable crystalline form (Perez, 2005). Other types of crystalline structures exist, although none of them are of the same technical importance as Cellulose I and II.

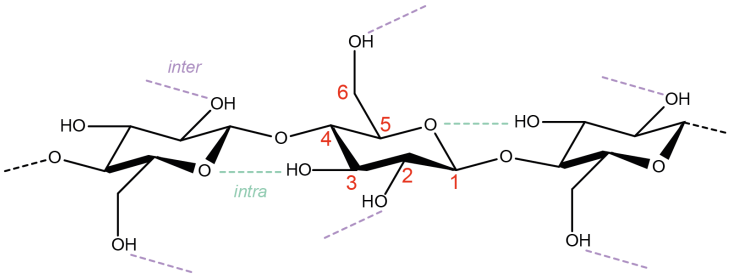

Figure 3. The molecular structure of cellulose, including intra- and intermolecular hydrogen bonds, with the hydrogen bond pattern of cellulose II.(Heinze *et al.*, 2012)

Cellulose is, however, not purely crystalline, neither in its native state nor in spun cellulose fibers. The cellulose is arranged in semi-crystalline microfibrils, with alternating crystalline and less-ordered parts. One cellulose chain can run from one microfibril to another, and the morphology is often referred to as the "fringed fibril model" (Klemm *et al.*, 2005). In the native state, these microfibrils are further aggregated into macrofibrils, and those are arranged in the layers of the cell walls of plants.

2.1.3 Technical lignin and cellulose pulp

As discussed in previous sections, valorization of lignin and/or cellulose from biomass, such as wood, requires separation. The separation process will influence the structure of the different components, and consequently also the properties of any subsequential processes and final materials. Two main types of available technical lignin are isolated from the two major chemical pulping methods: sulfite and sulfate (*i.e.*, the Kraft process) (Sixta *et al.*, 2006). The lignin from the sulfite process has sulfonate groups incorporated into it and is, thereby, water soluble. This type of lignin is usually referred to as lignosulfonates. Kraft is the dominant pulping method, about 150 million tons of Kraft pulp are produced annually (FAOSTAT, 2019), and in Sweden the majority is made from softwood (Skogsindustrierna, 2019). The advantage of the Kraft process is that the pulp fibers, especially if made from softwood, are very strong (Sixta *et al.*, 2006). Considering that carbon fibers are targeted in the current work, softwood lignin is also more reactive than hardwood, as it is mainly composed of guaiacyl units. This complicates melt spinning, as softwood lignin has low thermal stability (Baker & Rials, 2013). However, this feature is an advantage during the stabilization step (see Section 3.1) (Norberg *et al.*, 2013), and is beneficial to the carbon yield (Trogen *et al.*, 2021). In this work, a softwood dissolving pulp and softwood Kraft lignin were chosen as raw materials, and will hereinafter be referred to as simply cellulose and lignin.

In the Kraft pulping method, wood chips are cooked at approximately 150 ^{o}C in aqueous sodium hydroxide and sodium sulfide in a digester. Under these conditions, lignin is degraded and the fragments are solubilized at the high level of pH. Cellulose is also partly degraded, and the cellulose chains undergo mass loss and reduced de-

gree of polymerization, from peeling and alkali hydrolysis respectively (Sixta *et al.*, 2006). In the digester, the major part of the lignin (90-95% (Gellerstedt & Henriksson, 2008)) will be dissolved in the cooking liquor, which is then referred to as black liquor. From the digester, the black liquor is led to the evaporation plant where water is removed. The resulting viscous black liquor is incinerated in the recovery boiler, and the remains, a salt smelt, are recovered to produce new cooking chemicals. This approach results in a rather low utilization of raw material in the overall process (40-55%), but at the same time, it renders a surplus of energy in a modern mill. However, the recovery boiler often limits the capacity of the mill. These issues, with the low material yield and the limited capacity of the recovery boiler, can both be improved by extracting a fraction of the lignin from the process for further utilization (Öhman *et al.*, 2007b). Lignin can be separated from the black liquor by lowering the pH level. This can be done in various ways. For instance, in the LignoBoost process, where the pH level is reduced using carbon dioxide. When the level of pH reaches 9-10, the lignin will precipitate from the black liquor. The precipitate is dewatered by filtration. The filter cake is, thereafter, re-suspended at low level of pH (pH 3 - 4) before final dewatering and washing in a second filtration step (Öhman *et al.*, 2007a).

The native lignin undergoes substantial modifications regarding structure and molecular weight during the Kraft process, and several chemical reactions occur simultaneously. Phenolic lignins are the most reactive; at alkaline conditions and high temperatures, they cleave off into the quinonemethide intermediate. In the presence of a strong nucleophile, which in the Kraft process are hydrosulfide ions (HS^-), the β-O-4 bond is cleaved, creating a new phenolic lignin, and so on.(Sixta *et al.*, 2006) The majority of the lignin is non-phenolic. The degradation of these moieties, cleavage of the β-O-4 bonds, will also proceed at these high temperatures and alkali concentrations, but at a lower reaction rate compared to the phenolic moieties. Due to the breakage of the β-O-4 bonds, phenolic groups are the foremost functional groups in Kraft lignin.

As mentioned, many other lignin reactions occur, and the structure of native lignin is highly modified. Lignin structures that are linked through carbon-carbon bonds, such as β-5 or 5-5, are stable during Kraft pulping, but the phenylpropane side chains in these structures may be either modified or removed (Gellerstedt *et al.*, 2010). Crestini *et al.* (2017) have found that about 70% of softwood Kraft lignin (the fraction of the lignin soluble in acetone) showed a very low content of native lignin side chains, and also exhibited a highly branched structure. Carbon-carbon bonds may also be formed during the later stages of the cook, *i.e.* through condensation reactions. Carboxyl groups are also introduced into the lignin structure, and these functional groups are more prevalent in the low molecular weight fraction (Gellerstedt & Henriksson, 2008). Furthermore, chromophores, which are highly conjugated compounds, are created, giving the pulp and the cooking liquor their dark brown color. Malodouros organosulfur compounds, such as dimethyl mercaptane (CH_3SCH_3), are also formed in the digester, giving the Kraft process its characteristic smell, and Kraft lignin contains a few percentages of sulfur (Sixta *et al.*, 2006).

2.1.4 Choice of solvent

There are fewer solvents to choose from for cellulose than for lignin, which means that cellulose limits the potential solvents for the co-spinning of lignin-cellulose precursor fibers. This is due to a difference in the structure of the two and the lower molecular weight (MW) of lignin than of cellulose. Several factors complicate the dissolution of cellulose: the high degree of polymerization, the vast number of hydrogen bonds between chains, and the hydrophobic interactions that stabilize the stacking of sheets (Olsson & Westman, 2013a). A solvent must thereby first of all break both hydrogen bonds and hydrophobic interactions in order to dissolve cellulose. Second, long polymer chains, especially rigid ones such as cellulose, do not undergo major entropic gain when dissolved. This fact limits the number of solvents to choose from, as it does for most polymers (Navard *et al.*, 2012).

Commercially available man-made cellulose fibers include, as mentioned previously, viscose and lyocell. Viscose is produced by a derivatization of cellulose with carbon disulfide (CS_2) into cellulose xanthate, which is thereafter dissolved in sodium hydroxide (NaOH). However, CS_2 is a known carcinogenic substance, *i.e.* chemicals and emissions must be controlled carefully during production (Liebert, 2010). Lyocell is the other main type of commercially available man-made cellulose fiber. In the lyocell process, cellulose is directly dissolved in N-methyl morpholine oxide (NMMO) (Klemm *et al.*, 2005). The main issue with the lyocell process is that NMMO is thermally unstable and stabilizers must be added during the dissolution of cellulose to prevent runaway reactions and cellulose degradation (Rosenau *et al.*, 2002).

Ionic liquids have been identified as promising and safe solvents for cellulose, and this class of solvents offers many options. Ionic liquids are organic salts with a melting point below 100 °C; many of them are interesting because of their ability to dissolve cellulose at low temperatures, and they are temperature stable (Hermanutz *et al.*, 2018). For cellulose, the main dissolving effect of ionic liquids is proposed to come from the anion, which creates new hydrogen bonds with cellulose, thereby, separating the cellulose chains (Idström *et al.*, 2017). The separation is enhanced by the, often bulky, cation, which strives to maintain electric charge neutrality (El Seoud *et al.*, 2020). Different ionic liquids render solutions with very different rheology and, consequently, the choice of solvent affects the potential to spin cellulose fibers (Kosan *et al.*, 2008; Hauru *et al.*, 2016).

It is most likely that an even larger share of the ionic liquids also efficiently dissolve lignin (Casas *et al.*, 2013). The dissolution of lignin in ionic liquids is, as for cellulose, highly dependent on the choice of anion (Pu *et al.*, 2007). Results from modelling of lignin dissolution have also indicated that lignin moieties exhibit π-stacking with imidazolium cations (Janesko, 2011; Zhang *et al.*, 2017).

In the present investigation, cellulose and lignin were dissolved in the ionic liquid 1-ethyl-3-methylimidazolium acetate (EMIMAc), see Figure 4. EMIMAc is a liquid at room temperature, and the solvent has been extensively used in cellulose fiber

spinning studies (Kosan *et al.*, 2008; Olsson & Westman, 2013b). EMIMAc can dissolve high amounts of both lignin and cellulose at low temperatures. EMIMAc is more stable than NMMO, however, there is a risk of both cellulose and solvent degradation if solutions are stored for hours at higher temperatures (Michud *et al.*, 2015; Clough *et al.*, 2015).

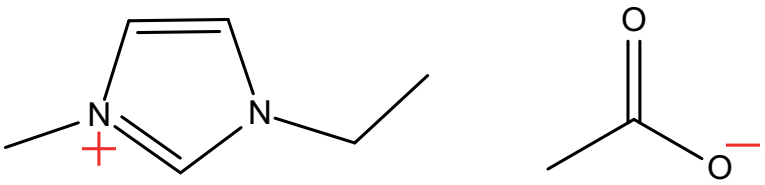

Figure 4. The molecular structure of EMIMAc.

A crucial part of the industrialization of a spinning process is recycling of the solvent. In the NMMO process, >99% of the solvent is recycled (Klemm *et al.*, 2005). There is currently no efficient way of recycling EMIMAc or other ionic liquids; however, ongoing research is investigating a number of recycling alternatives, such as freeze crystallization (Liu *et al.*, 2018), and evaporation (Elsayed *et al.*, 2020). In summary, there are currently no problem-free solvents for cellulose. Therefore, despite the current lack of recycling, ionic liquids are regarded as suitable direct solvents for dissolving and spinning cellulose and/or lignin, such as in the present study.

2.2 Spinnability

Air-gap spinning has advantages from both melt spinning and wet spinning, with the ability of coagulating a molecularly oriented fiber. However the spinning technique also exhibits limitations from both. Instabilities in the air gap can limit the degree to which an extruded solution can be stretched, the so-called draw ratio, during spinning. Thus, the maximum attainable draw ratio is often used as a measure of spinnability, *i.e* spinning performance (Hauru *et al.*, 2016). When using new, or new combinations, of raw materials such as in this work, it is important to analyze how the solution behaves and subsequently evaluate the spinnability of the solution. This can be done by characterization of the solution, with for example rheology, and identification of instabilities during spinning, and by considering the force balance to estimate the stress in the fibers during spinning.

2.2.1 Rheology

Rheological measurements provide the stress response of a fluid when it is subjected to mechanical deformation, *i.e.* strain. For a solid, elastic material, the stress response for small values of strain is independent of rate of strain, often called shear rate, but dependent on the magnitude of strain. In contrast, the stress response of a viscous fluid, again valid for small strain amplitudes, is strongly dependent on shear rate while stress is independent of the magnitude of strain. Materials that show both elastic and viscous behavior are called viscoelastic. Viscoelasticity also means that the fluid can store energy, under shear or elongational deformation. After the stress is released, the fluid relaxes towards its original shape. A purely viscous solution will dissipate all energy under shear and will not relax after stress has been recovered (Macosko, 1994). Polymer melts and homogeneous polymer solutions, including solutions of lignin and cellulose, are normally viscoelastic.

As mentioned, at small strains, the viscosity of a fluid only depends on shear rate, not on the magnitude of strain. This dependence is referred to as the linear viscoelastic region. However, if the strain increases, the viscosity will also depend on strain. Within the linear region, the complex viscosity measured with an oscillating deformation is analogue to the shear viscosity measured for rotational deformation; this is known as the Cox-Merz rule (Cox & Merz, 1958).

When shear is applied to a polymer solution, some of the chains will orientate in the shear direction, which lowers viscosity. But at low shear rates, other polymer chains might have time to relax and entangle, which leads to a constant viscosity for low shear rates. This is often referred to as a Newtonian plateau. The value of the viscosity of this plateau, or simply the viscosity at very low shear rates, is denoted zero-shear viscosity and can be calculated if the viscosity is extrapolated to 0, the "zero-shear rate". The magnitude of the zero-shear viscosity is dependent on tyoe of polymer, the polymer concentration, the molecular weight and type of solvent. Zero-shear viscosity at a certain temperature can be calculated by, for example, fitting the complex viscosity to the Cross Model. If the viscosity at infinite shear

rates, η_∞, is set to zero, the Cross Model becomes Equation 2 (Macosko, 1994). In Equation 2, η is the complex viscosity, η_0 is the zero-shear viscosity, K is a time constant, $\dot{\gamma}$ is the shear rate, and n is a power-law exponent.

$$\eta\left(\dot{\gamma}\right) = \frac{\eta_0}{1 + \left(K\dot{\gamma}\right)^{1-n}} \tag{2}$$

At a critical shear rate the polymer chains no longer have time to relax, resulting in a net orientation of the chains and a lower viscosity. Solutions with higher polymer concentrations and/or higher average molecular weight show the onset of shear thinning at lower shear rates (Meister & Kosan, 2015).

The modulus is also an important property for a viscoelastic solution; it is comparable to the shear modulus of an elastic material. The modulus is only dependent on shear rate within the linear range. Linearity means that if the strain varies sinusoidally, the stress response will oscillate at the same frequency as the strain (γ_0). For an elastic material, the stress response is in phase with the oscillating strain; as an ideal elastic material responds instantly to deformation. However, in viscoelastic materials where some energy is dissipated, the stress will be out-of-phase with the strain at a certain phase angle, (δ). The stress can, thereby, be divided into two components: one that is in phase with the strain (τ') and one that is out-of-phase by 90°. (τ''), as illustrated in Figure 5 (Macosko, 1994). Two moduli can be calculated from these two stress components, a storage and a loss modulus. The point at which the two moduli are of equal magnitude is called the cross-over point (COP). The magnitude of the moduli and the COP depends on the polymer concentration in solution and molecular weight distribution (MWD) (Meister & Kosan, 2015).

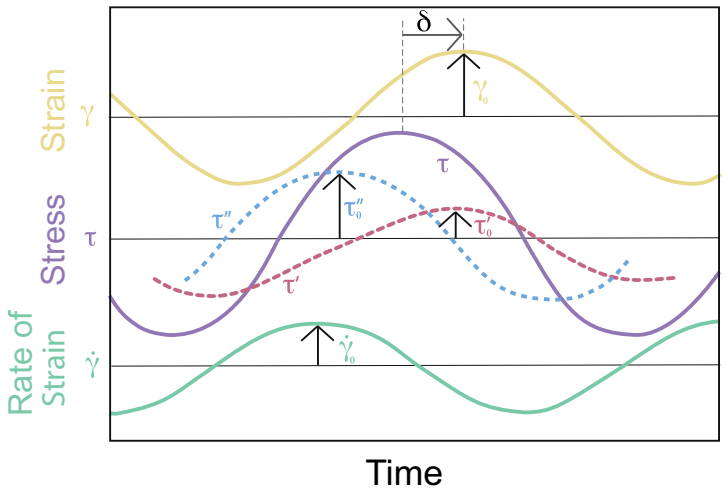

Figure 5. The stress response of a viscoelastic material where γ_0 is the applied strain and γ is the rate of strain, *i.e.* the shear rate. τ is the stress response where τ' and τ'' are the in- and out-of-phase components, respectively and δ is the phase angle. Reproduced from Macosko (1994).

Polymer solutions may behave differently in shear and extension (Petrie, 2006b), and thus evaluating the extensional behavior of polymer solutions is relevant for fiber spinning. Polymer solutions can be analyzed with Capillary break-up extensional rheology (CaBER), and the technique may give information on both extensional viscosity and relaxation time. Cellulose in EMIMAc has been analyzed with CaBER by Haward *et al.* (2012), however, at lower concentrations of cellulose than relevant for air-gap spinning. It is indeed difficult to find experimental set-ups suitable for concentrated polymer solutions (>10 wt%) to achieve useful data (Hummel *et al.*, 2015). One approach in measuring extensional viscosity is by pushing the polymer fluid through a hyperbolic die, creating an extensional flow, and measuring the volumetric flow rate for a specific pressure drop (Collier *et al.*, 2005). However, the set-up allows for only one magnitude of strain for each die, and offers no potential to estimate the influence of viscous and elastic effects.

2.2.2 Instabilities during spinning

Breakage of fibers can occur during spinning due to imperfections of the fluid, disturbances in the spinning set up, or can be caused by the limitation of the inherent properties of the fluid. The latter is known as critical breach, and a few types of critical instabilities during melt spinning are described in the scientific literature. In contrast, the mechanisms leading to spinning failure during wet spinning and air-gap spinning have not been as extensively studied. However, some analogies to air-gap spinning can be drawn from melt spinning since a concentrated polymer solution can, in many cases, be compared to a polymer melt (Wirth *et al.*, 2011). The application of an external force is required to extend and shape a viscoelastic fluid into a fiber, as is done during spinning. This force is balanced by viscous and elastic forces that develop in the deforming fluid. The fiber will break when an elastic force divided by the cross-sectional area equals the breaking stress (Ziabicki & Takserman-Krozer, 1964). This breach is known as cohesive break-up. A colder polymer melt with higher viscosity needs a stronger pulling force to be elongated, and will, therefore, break at lower draw ratios (Laun & Schuch, 1989; Demay & Agassant, 2014).

Other types of instabilities have also been identified during melt spinning: *e.g.* draw resonance. Draw resonance is a periodic fluctuation in diameter that grows substantially above a critical draw ratio, which is caused by perturbations on the spin line, such as variations in viscosity or extrudate dimensions (Petrie & Denn, 1976; Rauwendaal, 2014). If the amplitude of the fluctuation becomes large enough, it can split the fiber into droplets. On the other hand, a breach can also occur at the narrow cross sections, the formed nodes of the fiber, which break when they cannot bear the force (Wirth *et al.*, 2011). What decides when or why the spin line enters this unstable state is, however, not fully known.

Draw resonance has been observed at lower draw ratios in melt spinning if the cooling was applied in a rapid manner, for instance, when using a water bath (Petrie & Denn, 1976), This is of course very similar to the spinning path in air-gap spinning, and

draw resonance has been observed for air-gap spinning of cellulose-NMMO solutions (Navard & Haudin, 1985). The length of the air gap seems to play a role in the onset of draw resonance. Mortimer & Peguy (1996) have reported that the draw resonance was attained at higher draw ratios if the air-gap was extended. The explanation was that the velocity profile then had time to stabilize. However, Ishihara & Kase (1976) found that draw resonance could be suppressed if the air-gap was shortened when performing water-quenched melt spinning. Furthermore, the surface tension of a polymer solution is often neglected and not considered when air-gap spinning is discussed, but simulations of melt spinning indicate that surface tension destabilizes spinning and might play a part in inducing draw resonance in the system (Bechert & Scheid, 2017).

2.2.3 Force balance

The extruded fiber is under tension since:

$$v_0 < v_t \quad D_R = \frac{v_t}{v_0} \tag{3}$$

Where v_0 is the extrusion velocity, v_t is the take-up velocity, and D_R is the draw ratio.

The take-up force F_t, consists of frictional force, F_f, which arises from pulling the fibers through the coagulation bath, and a resisting force, F_r, as a result of stretching the solution in the air gap, as shown in Equation 4.

$$F_t - F_f = F_r \tag{4}$$

At the end of the air-gap, the resisting force is a sum of several forces, see Figure 6 (Ziabicki, 1976).

$$F_r = F_{rheo} + F_i + F_s - F_g \tag{5}$$

F_{rheo} is the rheological force, depending on the viscosity and the elasticity of the fluid, F_s arises from surface tension, F_i is the inertia it has to overcome and F_g is the push from gravity caused by vertical spinning.

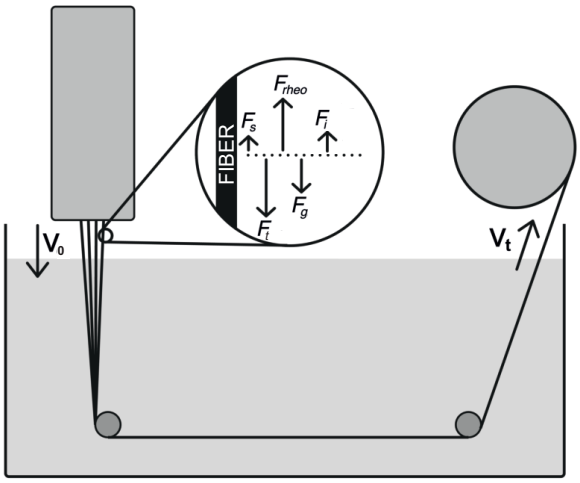

Figure 6. Force balance in the air-gap during extrusion.

If the radial distribution, $R(z)$, *i.e.* the shape of the extruded fiber, is not known, the contributions from inertia, surface tension, and gravity can then be estimated with the expressions from Ziabicki (1976). Gravity will only matter in the air gap since the coagulation bath (water) and the fiber have similar density, and thus the contribution to the overall force balance is minor. The radius of the fiber at the end of the air-gap, R_t, can be calculated from the radius at extrusion, R_0, using the equation of continuity.

$$R_t = \frac{R_0}{\sqrt{D_R}}$$

$$F_i = \rho Q(v_t - v_0)$$
$$F_i = \rho Q v_0 \left(D_R - 1\right)$$

$$F_s = \pi\sigma(R_0 - R_t)$$

$$F_s = \pi\sigma(R_0 - \frac{R_0}{\sqrt{D_R}}) \tag{6}$$

Where ρ is the density of the spinning solution, Q is the volumetric rate, and σ is the surface tension. And, F_g is the mass of the solution in the air-gap times the acceleration of gravity, $g = 9.81 m/s^2$.

$$F_g = \rho_S V_{airgap} g \tag{7}$$

The volume, V_{airgap} can, in this case, be simplified to a truncated cone with a base

radius of R_0 and a top radius of R_t with height L.

The frictional force from pulling the fibers through the coagulation bath depends on the velocity and the total surface of fibers in contact with the coagulation bath (length and radius). The frictional force can be calculated according to Equation 8 (Ziabicki, 1976; White & Hancook, 1981), if assuming that all elongation occurs in the air gap (Mortimer & Peguy, 1996), which results in a constant velocity and radius through the coagulation bath. The tow is also approximated to one large fiber, R_L.

$$F_f = 2\pi R_L L_c \frac{1}{2} \rho v_L^2 C_f \tag{8}$$

Where R_L is the approximated radius of the fiber tow, L_c is the length of the coagulation bath, ρ and μ are the density and viscosity of water, respectively. v_L is the fiber velocity, and C_f, the skin-friction coefficient, which can be estimated using (Ziabicki, 1976):

$$C_f = A \cdot Re^{-x} \quad Re = \frac{\rho v_L 2R_L}{\mu} \tag{9}$$

$$R_L = n\frac{R_1}{\sqrt{D_R}} \tag{10}$$
$$v_L = v_e \cdot D_R$$

In Equation 9, Re is the Reynolds number. In Equation 10, n is the number of fibers, R_1 is the fiber radius at a draw ratio of 1, and D_R is the draw ratio. Thus, by performing measurements and varying both coagulation bath length, L_c, and draw ratio, D_R, an expression for $F_f(D_R)$ can be obtained and subsequently the resisting force can be isolated from the take-up force.

3 Lignin valorization

Lignin constitutes the largest bio-based reservoir of aromatic compounds and has received a lot of attention in efforts to develop new products, chemicals, and fuels (Ragauskas *et al.*, 2014), and there are some commercial products. For example, lignosulfonates rendered from the sulfite process (about 5% of all chemical pulping (Sixta *et al.*, 2006)) are used as a dispersing agent and can also be converted into vanillin, which is commercially done by *e.g.* Borregaard, Sarpsbourg, Norway (Calvo-Flores & Dobado, 2010). Many different ongoing research activities are exploring potential applications for lignin. For instance, it may be possible to use lignin as feedstock for other chemical compounds. After lignin has been depolymerized, it can be converted either chemically or biologically into fine chemicals. The greatest challenge with this route is combining the polydispersity of lignin with the demand of high purity of the formed compounds (Ragauskas *et al.*, 2014). It can also be argued that it is better, more resource efficient, to utilize the whole lignin molecule. Even though native lignin is degraded during for instance the Kraft process it is still a macromolecule. Lignin molecules may be functionalized and used in or as thermoset resins and thereby reduce the need for non-renewable raw materials. However, also in this case the polydispersity of lignin is a challenge (Wang *et al.*, 2020). In terms of fiber development, lignin has also been blended with cellulose and cellulose derivatives with the aim of recreating wood. The ambition was that the addition of lignin would strengthen the cellulose fibers, however, this was only achieved when cellulose was spun from a few solvents and at a very low lignin concentration (Glasser *et al.*, 1996). Regarding fibers, lignin has mainly been spun by itself or blended with other polymers in the endeavour to create bio-based carbon fibers. The idea of making carbon fibers from lignin has been debated back and forth during the past decades. Lignin was identified as an attractive carbon fiber precursor due to its aromatic structure, as it results in a high carbon content (Gellerstedt *et al.*, 2010).

3.1 Lignin-based carbon fibers

Carbon fibers have unique physical properties, such as high specific strength and modulus, creep resistance, and chemical inertness. This combination makes them ideal materials in many construction applications (Morgan, 2005b). Carbon fibers are available with a wide range of mechanical properties as the strength and stiffness of the final carbon fiber depends on production parameters, both during fiber spinning and carbonization. Carbon fiber production has increased by more than 10% annually for over a decade, and in 2018, the annual production surpassed 100 thousand tons (The Fiber Year, 2019).

Carbon-fiber-reinforced composites can replace traditional construction materials, such as steel, and, thereby reduce the weight and environmental impact, for example, of the rotor blades of electric windmills, concrete, and vehicles (Mainka *et al.*, 2015). Commercial carbon fibers contain $> 92\%$ carbon, are less than 10 µm in diameter, and are produced as continuous fibers. They are traditionally produced in three main steps: spinning a precursor fiber, stabilization, and finally carbonization. Stabilization is performed in air at around 200-300 °C and is done to prevent the fusion of the precursor in the following step, and increases the final carbon yield. In the carbonization step, the stabilized precursor is heated in an inert atmosphere up to 1000 °C, or even higher. During this last step, the precursor is deoxygenated, and aromatized/cross-linked until basically only carbon remains in the molecular structure (Frank *et al.*, 2014).

It was in the 1960's that the interest in carbon fibers really started to grow. The primary reason was to supply new materials for space applications. Japanese researchers were the first to carbonize polyacrylonitrile (PAN), which soon became the preferred raw material and still is the main precursor for carbon fiber (Morgan, 2005a). PAN is dissolved in a polar, often organic, solvent and wet spun into precursor fibers. In the following thermal treatment, PAN undergoes dehydrogenation, cyclization, and coalescence of these cyclic structures, and the yield is around 50 %. By controlling the thermal processes, the properties of the carbon fibers can be tuned: lower carbonization heating rates promote higher tensile strength while very high temperatures, up to 3000 °C, result in high-modulus fibers (Frank *et al.*, 2014). PAN-based carbon fibers have excellent mechanical properties, 4-6 GPa in tensile strength (TS) and from 200 up to over 500 GPa in tensile modulus (TM) (Morgan, 2005b). However, PAN-based carbon fibers have two major drawbacks; they are very expensive, and consequently they are limited to applications where cost is not a major factor, and they are fossil-based. In particular the automotive industry is looking for a low-cost carbon fiber. In a review by Baker & Rials (2013), the mechanical properties of carbon fibers for the automotive industry was targeted to TS of 1.72 GPa and TM of 172 GPa. Therefore, other precursors, preferably bio-based, are being, and have been, evaluated.

Before the use of PAN, the main precursor material was cellulose in the form of viscose fibers. Carbon fibers from cellulose are produced commercially even today, however with a very low market share. Through a "hotstretching" of cellulose, *i.e.*

stretching in approximately 2500°, it is possible to achieve very strong carbon fibers from cellulose: 3-4 GPa in TS and 500-700 GPa TM (Morgan, 2005a). However, not only is such stretching extremely expensive, cellulose fibers suffer substantial yield loss during carbonization, far beneath the theoretical carbon yield of 44.4%. This can create voids inside the fiber that are detrimental to the mechanical properties (Frank *et al.*, 2014). Different strategies have been applied to overcome this issue, such as low heating rates during carbonization and incorporating dehydration catalysts. Research on cellulose-based carbon fibers has been resumed in recent years, for example by Spörl *et al.* (2017), who have produced carbon fibers with TS 2.0 GPa and TM 86 GPa.

Apart from cellulose and PAN, several other materials have been tested as carbon fiber precursors (Morgan, 2005a). Some other types of carbon fibers have even been commercialized, and dry-spun precursors from lignin were produced for a few years in the 1960's under the brand Kayocarbon. However, these carbon fibers were not that strong, with less than 1 GPa in TS (Otani *et al.*, 1964). In the early 1990's, lignin-based carbon fibers appeared on the agenda once again (Sudo & Shimizu, 1992). At this time, cost was the main concern regarding the future of PAN-based carbon fibers, and lignin was an inexpensive and underutilized bio-resource that attracted attention (Ragauskas *et al.*, 2014). Melt-spinning of lignin was, at this time, the main route, however, melt-spun lignin fibers require a very long stabilization time to prevent fiber fusion and, so far, have not exhibited sufficient mechanical properties. The most successful efforts have reached values of about 1 GPa in TS (Baker & Rials, 2013). Pure lignin fibers can also be dry-spun, which has been performed by Jin *et al.* (2018), resulting in stronger fibers (TS 1.4 GPa and TM 98 GPa). Due to the poor mechanical properties of pure lignin-based carbon fibers, increasing effort has been put into co-spinning of lignin together with another polymer.

Lignin has been blended with several other polymers, mostly synthetic, in order to enable the production of strong but yet inexpensive carbon fibers (Liu *et al.*, 2015; Culebras *et al.*, 2018). Lignin and cellulose can be blended in a fiber spun with the viscose process (Otani *et al.*, 1964). By utilizing the lignin solubility in aqueous alkali it was a development of an existing process. Recently, lignin-cellulose has come a substantial step further in becoming an available carbon fiber. Stora Enso and the viscose manufacturer Cordenka are currently cooperating and producing lignin-cellulose fibers as bio-based carbon fiber precursors at pilot-scale (StoraEnso, 2020).

Air-gap spinning has also been identified as a potential method for spinning lignin-cellulose fibers (Lehmann *et al.*, 2012). The technique enables the use of a wide range of solvents and raw materials (Garoff *et al.*, 2015; Ma *et al.*, 2015; Olsson *et al.*, 2017; Vincent *et al.*, 2018; Trogen *et al.*, 2021). However, how lignin affects the processability of such fibers has not been investigated and there remain challenges to this system that need further investigation; such as improving the mechanical properties, leaching of lignin in the coagulation bath (Garoff *et al.*, 2016), and adhesion of the final carbon fibers (Garoff *et al.*, 2019; Le *et al.*, 2020). To render high-strength carbon fibers, the precursor fibers should be highly oriented,

and, consequently, the spinning process and fiber structure should be examined and further adjusted in order to obtain better mechanical properties.

4 Materials and Methods

This section briefly describes the materials and methods used in the appended papers. Detailed information on the equipment and chemicals used, and precise experimental protocols are available in **Papers I - V**.

4.1 Raw materials

Softwood Kraft lignin (Lignin) was used for fiber spinning in all papers as well as in the mass transport and solubility experiments in **Paper II**. This lignin was obtained from LignoBoost Demo (Bäckhammar, Sweden) and was produced with the LignoBoost process. Two retentate lignins were additionally used in **Paper I**, where different membranes were used to remove a part of the lower molecular weight (MW) molecules. The different lignins were produced using either a 5 kDa (RL5) or 15 kDa (RL15) MW cut-off. Retentate lignins were produced with ultrafiltration of the initial lignin; more information on retentate production can be found in **Paper I**.

Two different pulps were used for fiber spinning in **Paper I**: a softwood Kraft dissolving-grade pulp purchased from Georgia Pacific (Atlanta, GA, USA) and a fully bleached paper-grade softwood Kraft pulp provided by SCA Forest Products (Sundsvall, Sweden). The former was also used in the coagulation study in **Paper II** and for fiber spinning in **Papers III-V**. Information on purity and the degree of polymerization is presented in Table 1. The solvent for the dissolution of lignin and cellulose was consistently EMIMAc (95%), which was purchased from Sigma-Aldrich (Steinheim, Germany) and was used as received.

Table 1. Intrinsic viscosity and results from carbohydrate analysis of the pulps used.

Pulp type	Intrinsic viscosity / ml g^{-1}	Carbohydrate composition / mg g^{-1}			
		Glucose	Xylose	Mannose	Galactose
Dissolving pulp	465	860	27	19	0.5
Paper-grade pulp	630	730	64	52	2

4.1.1 Characterization of lignin and cellulose

The purity of the raw materials and spun fibers was analyzed with respect to carbohydrate and Klason lignin content after hydrolysis in 72% sulfuric acid. The solid residue after complete hydrolysis is defined as Klason lignin. The monomeric sugars in the solution were analyzed with high performance liquid chromatography Theander & Westerlund (1986). Lignin in solution, referred to as acid soluble lignin, was measured in a UV spectrometer at 205 nm.

Intrinsic viscosity, which gives an indication of the average MW, was determined for the pulp according to ISO 5351:2010 - "determination of limiting viscosity number in cupri-ethylenediamine solution". The MW distribution of lignin was analyzed with gel permeation chromatography (GPC). Lignin and lignin-cellulose fibers were mixed with the mobile phase (10 mM LiBr in DMSO). Regarding the fibers, the cellulose did not dissolve and formed a milky-white gel at the bottom of the vials. Consequently, all of the lignin was considered to be dissolved, and the supernatant was used for analysis.

4.2 Solutions of lignin and cellulose

Solutions were prepared in a similar manner throughout the whole work. The pulp was ground and the lignin sieved before mixing with the solvent, EMIMAc, to ensure good impregnation of the solvent during dissolution. Lignin powder was mixed in after the cellulose, which was easiest done stepwise, *i.e.* little by little with mixing in between, since the lignin otherwise tended to form tough clumps. The solution mixture was added to a closed reactor, heated to 70 °C, and stirred at 30 rpm using an anchor impeller. It is important to remove air from the solution prior to fiber spinning, since air bubbles can cause fiber breakage. Therefore, the solution was transferred to the container used during spinning, and deaeration was performed at 60 °C below 10 kPa pressure for at least 5 h.

4.2.1 Characterization of solutions

The quality of dissolution was observed using an optical microscope from Nikon Eclipse Ci-POL (Nikon Instruments, Tokyo, Japan). When a solution is placed

between two orthogonal polarizers, any non-dissolved fibers will be clearly visible, as they are birefringent.

The solutions were analyzed with oscillating rheometry on a CS Rheometer (Bohlin Instruments, Cirencester, UK) equipped with a cone/plate-geometry (25 mm/5°) and strain of 0.01, to obtain the temperature-viscosity relation for each spin dope. Master curves for the complex viscosity and shear moduli were created according to the time–temperature-superposition method described by Metzger (2014), and only the horizontal shift factor, a_T, was used. The zero shear viscosity was calculated by fitting the master curve of the complex viscosity to the Cross Model after η_∞ was set to zero, (using the Matlab Curvefitting tool) according to Equation 2.

Surface tension measurements were performed using the pendant drop method with an optical drop contour analysis, OCA 40 Micro (DataPhysics Instruments, Filderstadt, Germany). The temperature was controlled with a temperature chamber in combination with a temperature-controlled dosing system. Temperature was set to either 45, 60 or 75 °C, and measurements were performed until drop formation was finalized, which took up to 20 min for high viscosity solutions. The syringe had a diameter of 1.83 mm, and the drop contour was determined with the software SCA202 V.5.0.32 build 5032 (DataPhysics Instruments, Filderstadt, Germany). The density of the solutions was measured with a He-pycnometer AccuPycII 1340 (Micromeritics Instrument, Norcross, USA) at room temperature, and the temperature dependence was calculated according to: $\rho_{EMIMAc} = -0.00055T + 1.1209$. Based on the results of Schuermann *et al.* (2016) it was assumed that the density of cellulose solutions decreases with temperature with the same coefficient as EMIMAc.

The extensional behavior of the solutions was analyzed with Capillary Break-up Elongational Rheometry (Haake CaBER 1, Thermo Haake, Karlsruhe, Germany). The measurement setup comprised two circular plates with a diameter of 4 mm and an initial separation of 2 mm. For successful sample loading, the two plates were heated to 75 °C. The plates were separated at time t = -50 ms, with a linear velocity profile until time t = 0 s, to a final gap of 6 mm. The diameter of the liquid thread at the midplane between the two plates was monitored with a laser micrometer at a frequency of 10 Hz and with a detection limit of 10 µm.

4.3 Fiber spinning

The solution was spun in a bench-scale spinning instrument, which consisted of a piston spin pump, a spin bath, and take-up rolls, see illustration of the setup in Figure 7. Extrusion was performed with a multi-fiber die, see details of the different die geometries in the appended papers, and extrusion generally progressed with less smudging of the die outlet if the solution was colder. During spinning start-up, the air gap was several centimeters in order for the solution to exit without wetting the die. When extrusion was stable, the air gap was reduced to 1 cm. It was

found that a higher draw ratio could be attained if the coagulation bath was cold, preferably around 5 °C. This observation is also in line with previous findings for similar solvent systems (Hauru *et al.*, 2014; Michud *et al.*, 2016) and could be due to a stronger semi-coagulated fiber when the coagulation bath temperature is lower, or perhaps a colder bath results in favorable conditions in the air gap that limit die swell (Mortimer & Peguy, 1996). The lignin-cellulose fibers appeared much stickier than the pure cellulose fibers, and the take-up rolls had to be covered with Teflon to be able to collect the fibers. The fibers were, thereafter, washed in deionized water for 24 h and subsequently dried at 80 °C for 45 min. By treating the fibers with a cationic fabric softener (Neutral, Unilever) before drying, they became easier to separate from the tow into single fibers, and the softener also seemed to prevent the fibers from breaking up during drying.

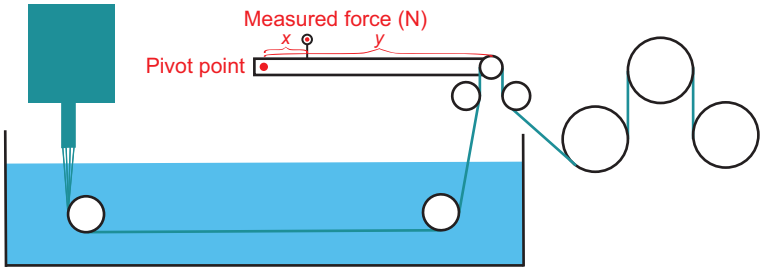

Figure 7. Sketch of spinning set-up, in this case including force measurement during spinning, which was only mounted when the take-up force was analyzed.

4.3.1 Stress in fiber during spinning

The take-up force was measured according to Figure 7. A die with 33 holes was used to achieve reliable force measurements. The take-up force measurement was only conducted as long as spinning was achieved, *i.e.* as long as fibers were formed from all capillaries in the die, and was thus aborted as soon as any fibers started to break.

The take-up force was calculated from the measured force according to:

$$F_t = \frac{F_m}{2l} \tag{11}$$

In Equation 11, F_t is the take-up force, F_m is the measured force, and l is the leverage (y/x in Figure 1).

The take-up force is a result of the resisting force from stretching the solution, and the friction from pulling the fiber tow through the coagulation bath:

$$F_t = F_r + F_f \tag{12}$$

To evaluate the different contributions to the resisting force, inertia and surface tension forces were estimated with Equation 6. These forces were found to be of little importance. However, surface tension might be of importance at high draw ratios close to the critical draw ratio, but this is a difficult point to measure as the measured force become invalid as soon as some fibers starts to break. Since the air-gap was only 1 cm and the density difference between the solution and coagulation bath, water, is small, the gravitational force was neglected (White & Hancook, 1981). Thus, the resisting force was estimated to be equal to the rheological force:

$$F_r \approx F_{rheo} \tag{13}$$

The frictional force, F_f, was estimated by spinning in coagulation baths of different lengths (0.24, 0.3, 0.4, and 0.5 m) and with four different draw ratios (1, 4, 8, and 10) for the solution L50C8 at 60 °C, see take-up force versus coagulation length in Figure 8. The particular solution and temperature were chosen to enable a high number of possible draw ratios. The data was used to determine the constants A and x in Equation 14, obtained by combining Equation 8 - 10, see Figure 9. An expression for friction as a function of the draw ratio was thereby obtained. It was assumed that all stretching took place in the air gap, i.e the fiber had a constant velocity throughout the coagulation bath (Mortimer & Peguy, 1996). Regard was taken to the different fiber radius for the different solutions, due to their different polymer concentration.

$$F_f = 2^{-x} A\pi \left(nR_1\right)^{1-x} \rho^{1-x} v_0^{2-x} \mu^x L_c D_R^{1.5-0.5x} \tag{14}$$

In Equation 14 n is the number of fibers, R_1 is the fiber radius at a draw ratio of 1, ρ and μ are the density and viscosity of water (the coagulation bath) respectively, v_0 is the extrusion velocity, L_c is the coagulation length and D_R is the draw ratio. A was determined to be 79.3 and x to be 0.66.

The estimated friction was then subtracted from the take-up force, according to Equation 4, and by using the assumption made in Equation 13, the stress in the fibers was calculated according to Equation 15.

$$\sigma = \frac{F_r}{A} = \frac{F_r D_R}{\pi R_e^2 n} \tag{15}$$

In Equation 15, σ is the stress in the fiber, R_e is the radius of the extruded fiber, D_R is the draw ratio and n is the number of fibers.

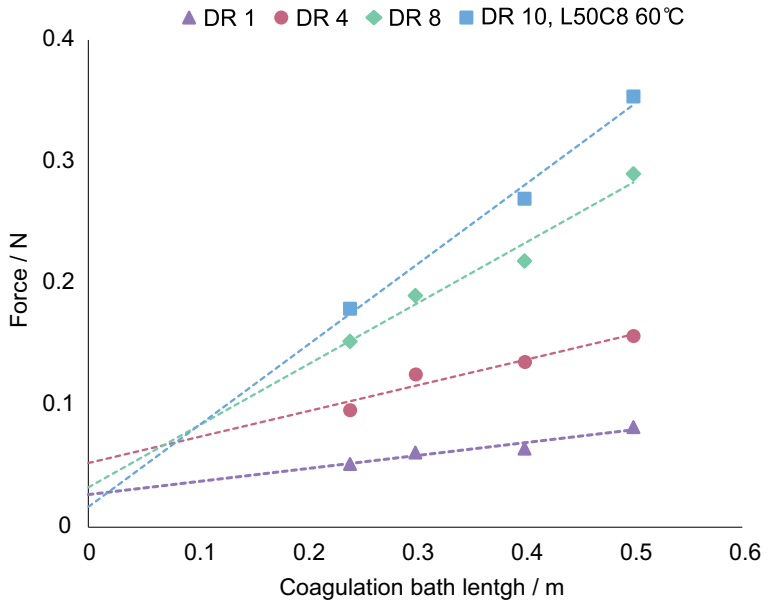

Figure 8. Take-up force during spinning of L50C8 at 60 °C with different lengths of the coagulation bath and draw ratios, with a linear regression of the data extrapolated to a coagulation length of 0 m.

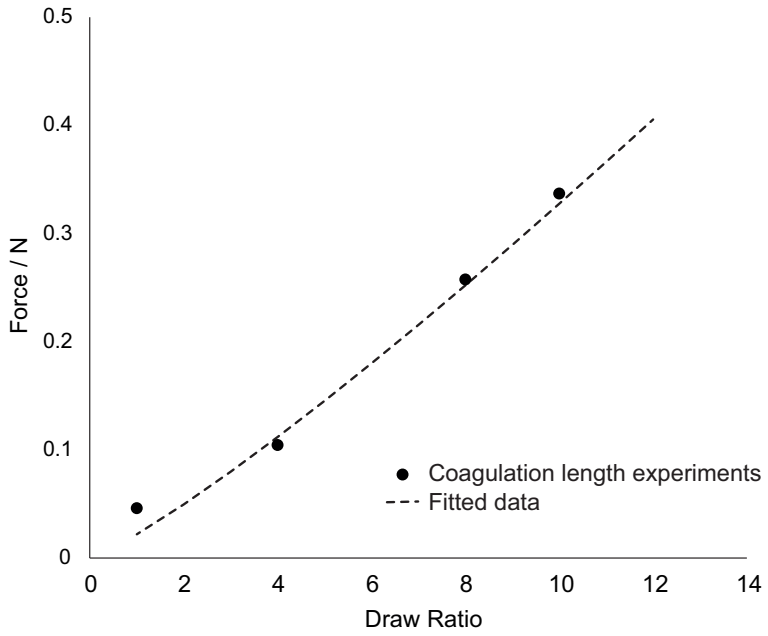

Figure 9. Friction extracted from the coagulation length experiments and data fitted to Equation 14

4.3.2 Evaluation of breach mechanism

The air gap was photographed and recorded during spinning to be able to analyze the mechanisms causing fiber breach. By using a Makro lens on a digital camera, the magnification and resolution were high enough to calculate the die swell of the extruded fibers. Die swell was calculated by dividing the maximum thickness of the extruded fiber with the capillary diameter. The air gap was also recorded with a high-speed video camera (500 frames per second) equipped with an "End trigger" function enabling the capture of fiber breach. The slow-motion videos enabled the identification of the location of the breach and any diameter fluctuation (draw resonance) preceding the breach. In total, 10-12 videos were collected for each temperature and were evaluated anonymously by three persons separately. The films were then rated with a score of 1 for a clear draw resonance and a score of 0.5 if a tendency for draw resonance was present.

4.4 Mass transport during coagulation

Mass transport during the coagulation of a lignin-cellulose fiber includes the inward diffusion of water, the diffusion of EMIMAc out of the fiber, and the leaching of lignin. Membrane coagulation was applied as a model system for fiber coagulation and is illustrated in Figure 10. The method is described in detail in a publication by Hedlund *et al.* (2017). In short, a well-defined tube-shaped membrane was coagulated in a stirred coagulation bath with known mass. The residence time in the coagulation bath was varied from 3 s up to 72 h to cover the whole course of coagulation. After removal from the coagulation bath, the membranes were put in new vials filled with deionized water, denoted washing baths, and were left for at least 3 days to reach apparent equilibrium.

Three different conditions in the coagulation bath were investigated: acidity and solvent content (15% EMIMAc), and a combination of the two. Pure MilliQ-water was used as the reference. A coagulation bath containing EMIMAc was included since this situation would occur in industry, which utilizes counter-current washing of fibers. To limit the energy demand during solvent recovery, the solvent content should be as high as possible (White, 2001), and 15% EMIMAc was chosen accordingly. The acidic coagulation baths contained either acetic acid or sulfuric acid.

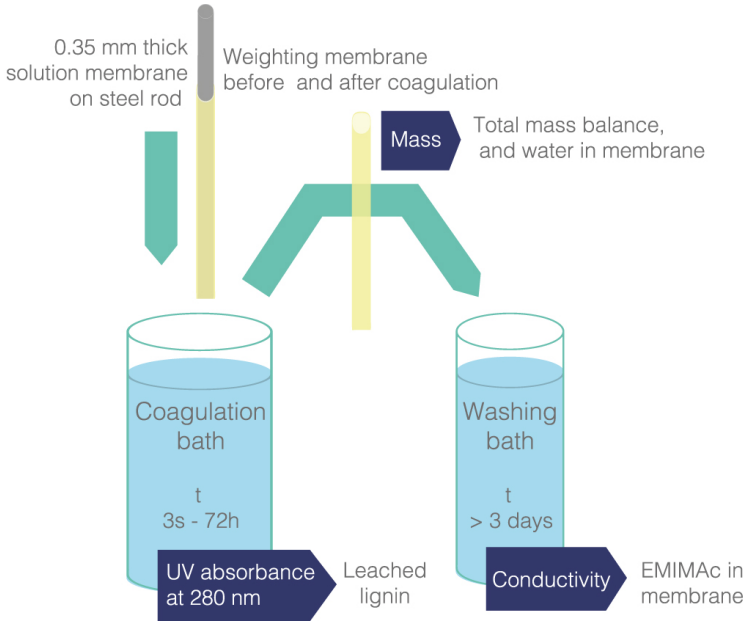

Figure 10. Illustration of the membrane coagulation method, including the analytical tools used.

Leached lignin was quantified with UV absorbance at 280 nm and the efflux of EMIMAc was determined from the amount of EMIMAc that remained in the membrane after a certain time, given by the concentration of EMIMAc in the washing bath, which was measured with conductivity. Apparent diffusion coefficients were calculated using the same methodology as applied by Hedlund *et al.* (2017). For short times, the time range used was $15 < t_i < 240$ s, the EMIMAc concentration adjacent to the steel rod can be considered constant, and the coagulation can be described by the equation of Fickian diffusion into an infinite slab in a single dimension, see Equation 16.

$$\frac{\partial c}{\partial t} = D\frac{\partial^2 c}{\partial x^2} \tag{16}$$

In Equation 16, c is the concentration, x is the distance from the solution-coagulation bath interface in meters, and D is the diffusion coefficient in $m^2 s^{-1}$. By using the boundary conditions clarified by Hedlund *et al.* (2017), the final diffusion coefficients were calculated as the average of the time range used, according to Equation 17.

$$D_i = \frac{\pi}{t_i}\left(\frac{M_i(t)}{M_{tot}}\frac{d}{2}\right)^2 \tag{17}$$

In Equation 17, D_i is the diffusion coefficient calculated after a certain time in seconds, t_i, and d is the thickness of the membrane in meters corrected for the curvature of the membrane. $M_i(t)$ is the mass of EMIMAc transported out from the

membrane after time t_i, normalized against M_{tot}, which was the mass of EMIMAc transported out after 60 000 s.

4.5 Characterization of fibers

The linear density, often called titer, of fibers was measured with a Vibroskop (Lenzing Instruments, Lenzing, Austria). This device determines the linear density in *tex* by inducing a vibration and, thereafter, changing the length of the free fiber until resonance is obtained. When the titer is known, the tenacity and elastic modulus (both in *cN/tex*) can be measured with a Vibrodyn (Lenzing Instruments), which performs a tensile stretch of the fiber until breakage. The results from tensile tests of polymeric fibers are highly affected by humidity. Therefore, all measurements were done in a controlled climate of 21.5 °C and 65% RH. The mechanical properties could be converted into SI units, by measuring the density of the fibers with a pycnometer and assuming a circular cross section.

Birefringence was measured with a Nikon Eclipse Ci POL, polarized light microscope with a 3λ Berek compensator. The thickness of the fiber was calculated from the linear density in dtex, density of the fiber and assuming a circular cross section. The pure cellulose fibers were assumed to have a density of 1.5 g/cm^3 (Sixta *et al.*, 2015). The density of the fibers with 67 % lignin was measured with a He-pycnometer, AccuPycII 1340 (Micromeritics Instrument, Norcross, USA) at room temperature. The density of fibers with other lignin ratio was thereafter calculated from a linear regression of these data. The birefringence, Δn, was calculated as the ratio between the retardation of the polarized light for maximum darkness divided by fiber thickness.

Scanning Electron Microscopy (SEM) was used to observe the surfaces and cross sections of fibers. A high vacuum is needed to receive high-resolution images. However, since lignin-cellulose fibers are poor electrical conductors, there is often a problem with charging and image distortion as well as beam damage. This problem could partly be avoided by coating each sample with 1-1.5 nm of platinum and lowering the accelerating voltage applied to the electron beam. Images were captured with a SEM from JEOL, model JSM-7800F. Secondary electrons and back-scattered electrons images of fiber cross sections and top views of the lignin fiber surfaces were acquired typically using an accelerating voltage of 5 kV and a working distance of 10 mm.

Other analytical techniques used in the appended papers include rotor synchronized magic-angle spinning (ROSMAS) NMR spectroscopy. The method for the ROSMAS experiments is explained in detail in **Paper IV**. The ROSMAS experiment enables extraction of the molecular orientation within the fibers, and together with the chemical sensitivity of NMR, it allows for the analysis of cellulose and lignin separately.

5 Results and Discussion

5.1 Fiber spinning and critical draw ratio

As early as during initial trials, it was noted that solutions that contained lignin were more easily spun into fibers than pure cellulose-EMIMAc solutions. To analyze the impact of the addition of lignin to a cellulose solution on the spinnability of the solution, the critical draw ratio during spinning was investigated. The solutions used in the experiments are summarized in Table 2.

Table 2. Lignin and cellulose concentrations in the solutions.

Solution	Total polymer concentration, wt%	Lignin ratio, wt%	Cellulose concentraion, wt%
L0C8	8	0	8
L30C8	11.4	30	8
L50C8	16	50	8
L70C8	26.7	70	8
L0C11.4	11.4	0	11.4

Figure 11 provides the critical draw ratios for each solution at different temperatures. As can clearly be seen in the figure, a higher lignin ratio in the solution enabled a higher critical draw ratio. This increase in critical draw ratio may be explained by the higher polymer concentration of the solution, as this may enhance its breaking stress. On the other hand, the L30C8 and L0C11.4 solutions have the same polymer concentration, but L30C8, which contains lignin, attained a nearly twice as high maximum critical draw ratio, hereafter denoted maximum draw ratio. Accordingly, the addition of lignin to a cellulose solution had a beneficial effect on the maximum draw ratio.

When the zero-shear viscosity was analyzed, it was concluded that the solutions that contained lignin achieved their maximum draw ratios at lower zero-shear viscosities

than the pure cellulose solutions, as indicated in Figure 11. Conclusively, the addition of lignin to a cellulose solution enabled higher draw ratios, especially when solutions at lower viscosites were compared. Recent results from Protz *et al.* (2021a) on spinning of cellulose-lignin NMMO-solutions did not show this beneficial effect of the lignin, however, solutions with different lignin content were only compared within a narrow temperature range.

It is notable that all solutions exhibited a maximum in critical draw ratio, with the exception of L0C8 since no spinning was performed below 30 °C. The maximum draw ratio for L0C8 may well be attained at lower temperatures, as indicated from the results. The maximum draw ratio lead to the conclusion that the critical draw ratio is limited by two mechanisms, one that is dominant at lower temperatures and one at higher temperatures.

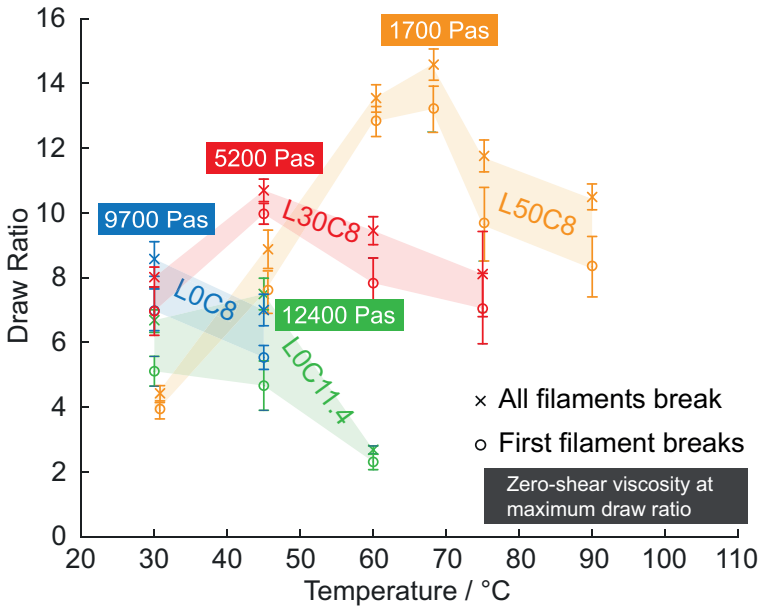

Figure 11. Critical draw ratio for each solution at selected temperatures. The shadowed areas are added to help guide the eye to the maximum draw ratio of each solution. The zero-shear viscosity of each solution at maximum draw ratio is indicated in the boxes.

In an attempt to elucidate the differences in spinnability, solutions were analyzed with oscillatory shear rheology at several temperatures (30 - 90 °C). In order to enable better comparison of the rheological behavior, master curves of the complex viscosity were generated from the measurements at different temperatures. The master curves at 45 °C are shown in Figure 12. Further analysis showed that the viscosity curves for solutions with the same amount of cellulose, L0C8, L30C8 and L50C8, may be shifted to complete overlap. This indicates that addition of lignin affects the overall viscosity in the same way as temperature in the studied frequency range. Viscosity measurements of 15% Kraft lignin in EMIMAc performed by Protz *et al.* (2021b) indeed exhibited pure Newtonian behaviour. The storage and loss

moduli of solutions were also similar when the solutions had the same zero shear viscosity, indicating no difference in viscoelastic behaviour between the solutions with and without lignin. The linear shear rheology, consequently, could not explain the difference found in spinning behavior between solutions with and without lignin, cf. Figure 11. The surface tension was also measured, available in **Paper V**, but neither those findings could explain the differences in spinnability.

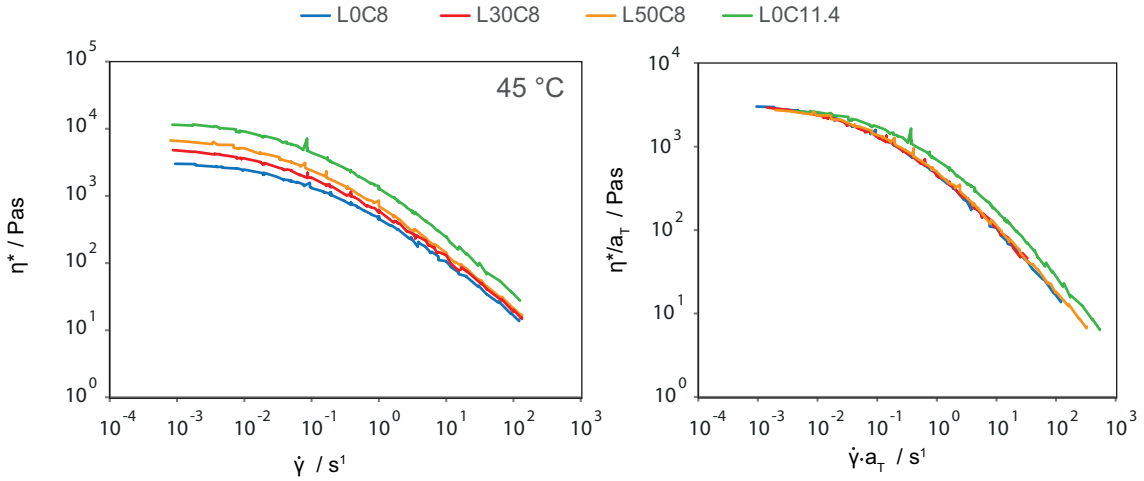

Figure 12. Master curves of complex viscosity for L0C8, L30C8, L50C8, and L0C11.4. In the right plot, the curves have been shifted to overlap according to time–temperature superposition (Metzger, 2014).

The decrease in critical draw ratio at colder temperatures, higher viscosities, could be due to die swell. A colder and thus more elastic solution can be expected to experience a more pronounced die swell and, subsequently, the true draw ratio might be higher. The extrusion was photographed and the die swell was calculated for the L50C8 solution at 30, 45, 60 °C, *i.e.* temperatures lower than the temperature of the maximum draw ratio. The results are available in **Paper III**. No difference was found for these three temperatures and, consequently, die swell was likely not the cause of the lower critical draw ratio at lower temperatures.

To further analyze the spinning process, the take-up force was measured to investigate the stress build-up with draw ratio for the different solutions. Data was collected from draw ratio 1 up to the critical draw ratio. The stress in the solution depends on the viscosity of the solution as well as on stored elastic stress. Elasticity is a memory effect; chains that are extended during the stretching want to move back into their original state. The faster the fluid is deformed, *i.e.* in this case at higher draw ratio, the fewer chains will have time to relax into their original shape. Thus, elastic stress will increase until all chains have reached their maximum elongated state. To extract an extensional viscosity, or perhaps try to isolate the viscous and elastic contributions on the stress would be very interesting. However, since there is no information on the shape, the radial distribution, of the extruded fiber and thus no extension rate, such calculations would require further assumptions. Therefore,

it was considered more useful to only compare the stress in the solutions (Petrie, 2006a).

In Figure 13, the stress is plotted versus the draw ratio for solutions spun at a temperature lower than the temperature of their maximum draw ratio, cf. Figure 11. As can be seen, the stress increased until the critical draw ratio was reached for all solutions. This data suggests that at temperatures lower than the temperature for maximum draw ratio (cf. Figure 11); the fibers undergo cohesive breakage, and they break once the breaking stress has been reached. However, it is difficult to determine a breaking stress from these data since the measured force becomes invalid as soon as a few fibers start to break.

When temperature increases, the force to extend the fiber decreases due to lower viscosity, and the breaking stress is reached at a higher draw ratio (Laun & Schuch, 1989), as was clearly found for solutions L30C8 and L50C8 at 30 compared to 45 °C in Figure 11.

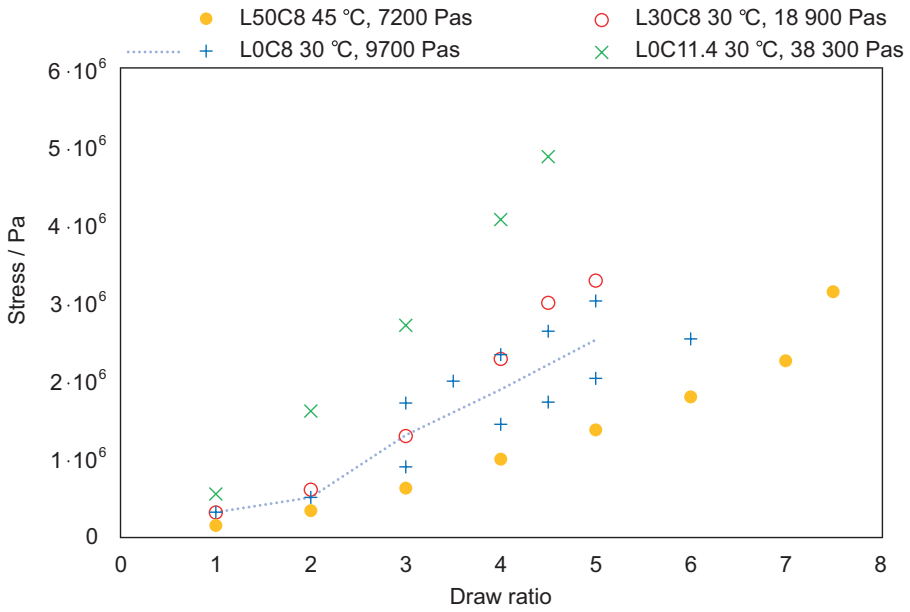

Figure 13. Calculated stress in fibers during spinning at lower temperatures. The dotted line is an average of the L0C8 data, added to guide the eye.

In Figure 14, the stress is plotted versus the draw ratio for solutions spun at or above the temperature of their maximum draw ratio, cf. Figure 11. Compared to Figure 13, all stress curves exhibit a different behavior, in this case a maximum stress is noted for all solutions, apart from L0C11.4. It is notable that fiber breakage does not occur at the maximum stress, which indicates another breaking mechanism than cohesive breakage. Such mechanism may be necking and/or draw resonance which causes a locally reduced cross section and thus stress amplification leading to fiber break-up.

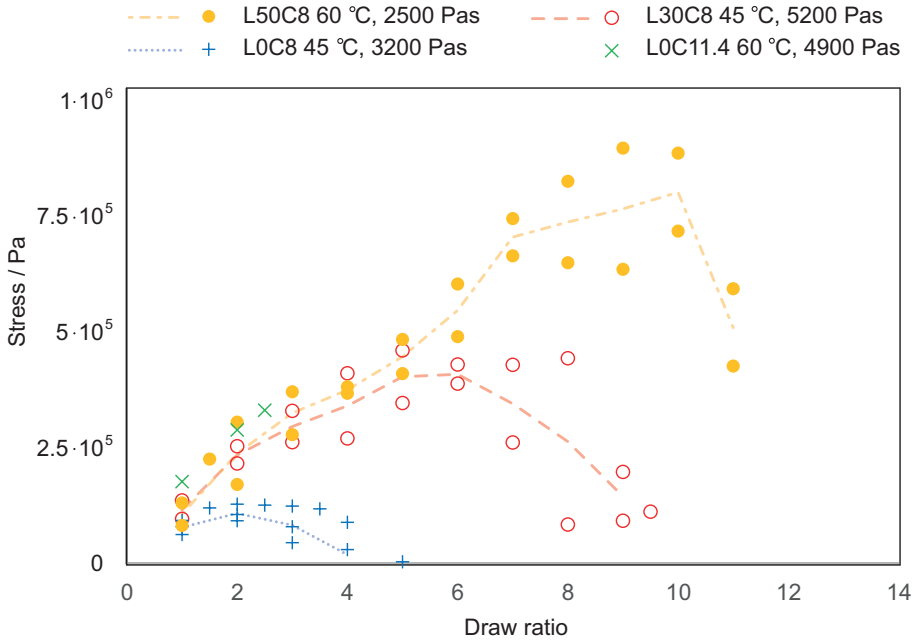

Figure 14. Calculated stress in fibers during spinning at higher temperatures. The lines are average values, added to guide the eye.

When analyzing the video recordings of the fiber breakage, the existence of a periodic fluctuation of the fiber diameter was noticed, *i.e.* draw resonance. Images captured from one video recording are shown as an example in Figure 15. A correlation with temperature was found, as can be seen in the graph in Figure 15, and the occurrence of draw resonance at breakage increased dramatically above 60 °C. The breakup at warmer temperatures was therefore assumed to be caused by necking and/or draw resonance.

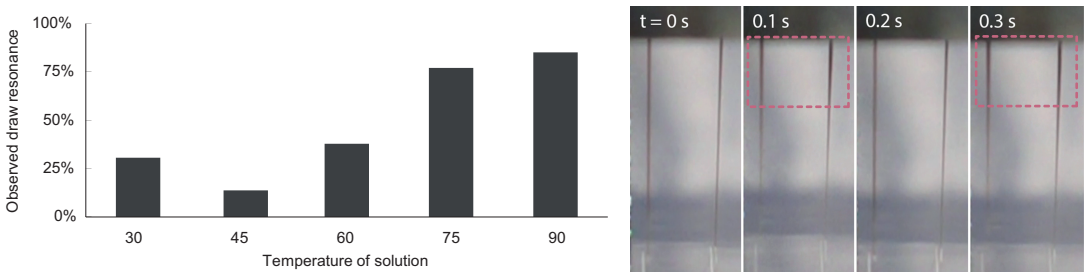

Figure 15. Left: Observations of draw resonance at different temperatures of solution. Right: Still photos captured from video recordings of spinning of L50C8 at 75 °C.

From the results presented above, it is evident that the addition of lignin stabilizes spinning at high draw ratios. Furthermore, the largest difference in critical draw ratio was found in the temperature region where draw resonance was observed. These results indicate that lignin stabilizes against diameter fluctuations. How lignin

enables this is not fully understood, but will be discussed below.

A maximum in the stress - draw ratio curve, as seen in Figure 14, could be interpreted as the point of an overall chain-chain slippage, which at a further increase in draw ratio will cause fiber breakage. Previous studies have found that the mechanical properties of pure cellulose fibers reaches a plateau at comparable draw ratios (Fink *et al.*, 2001; Sixta *et al.*, 2015; Elsayed *et al.*, 2021), indicating that an extended structure is achieved for pure cellulose fibers at low draw ratios.

The stress curves for the solutions containing lignin, L50C8 and L30C8, are different from L0C8. Some sort of a shoulder, more pronounced for L50C8, in the stress curve can be seen between 2 and 4 in draw ratio. Instead of turning downward as the L0C8 stress curve does, the L50C8 and L30C8 curves continues to rise. All three solutions have the same cellulose content and around draw ratio of approx. 3, all the cellulose chains may approach their maximum extendability.

A plausible explanation is that lignin interacts with cellulose and thus hinders cellulose chain slippage and in such a way enables an increase in stress in the solution. A notable difference between lignin and cellulose is their structure both regarding molecular weight, morphology, and molecular/chemical structure. The addition of lignin to the solution could thereby introduce additional hydrophobic interactions due to the aromaticity of lignin, and thus interact with cellulose in different ways than cellulose alone.

In summary, a solution that contain both lignin and cellulose enables a higher load at higher temperatures before breakage than a pure cellulose solution. It seems that lignin contributes with other interactions than cellulose alone, and that these enable an increase in elasticity and/or viscosity, which allows the total stress in the solution to increase; all in all that hinders cellulose chain slippage at high draw ratios. Further investigations of the spinning process, preferably *in-situ* analysis of the structure at the molecular level within the solution, are needed to fully understand the beneficial effect of lignin on spinnability.

5.2 Coagulation of lignin-cellulose solutions

One of the issues when spinning solutions that contain both lignin and cellulose is that a minor part of lignin is water soluble. This results in lignin leaching out into the coagulation bath. Leaching of lignin reduces the lignin content of the fibers and, consequently, the final carbon yield of the carbon fibers and should thus be limited. Lignin dissolved in the coagulation bath also must be considered during solvent recovery. For example, the major fraction of lignin could be removed with membrane ultrafiltration in a study on EMIMAc recycling (Liang & Liu, 2020).

To know the extent of the issue, it is important to analyze the coagulation process and identify the type and quantity of the leached lignin. The effect of leaching of lignin on solvent mass transport is also important because solvent mass transport controls appropriate residence times in the spinning process. The total mass transport was followed during coagulation in different coagulation baths and the lignin content in spun fibers was also analyzed. The used coagulation baths are presented in Table 3. The coagulation baths containing EMIMAc were included since this situation would occur industrially in a counter-current washing step of fibers, and the solvent content should be as high as possible to limit the energy demand during solvent recovery (White, 2001). Table 3 also includes the apparent solubility of lignin, and the fraction of lignin that dissolves after mixing with a certain coagulation bath, for both dry powder and lignin dissolved in EMIMAc. The two dissolution methods gave different apparent solubility values. The difference is likely attributed to that the lignin will having a higher solubility in a solution that also contains EMIMAc.

Table 3. Coagulation baths used, the soluble fraction of dry lignin powder and lignin dissolved in EMIMAc. Lignin refers to Softwood Kraft Lignin

Conditions in coagulation bath	**Soluble fraction of lignin (dry powder)**	**Soluble fraction of lignin (12 wt% lignin in EMIMAc)**
MilliQ water, pH 7	1.6% ± 0.4%	5.9% ± 0.5%
0.6% Acetic acid, pH 4	2.1%	6.2%
12% Acetic acid, pH 2.4	4.2%	10.0%
15% EMIMAc, pH 7	5.4%	13.0%
15% EMIMAc 12% Acetic acid, pH 4	13.3%	26.3%
Sulfuric acid, pH 2.4	1.1%	5.6%
Sulfuric acid, pH 1.3	0.9%	4.4%

Figure 16 presents the total mass transport during coagulation. The total mass of the membrane first increased due to an influx of water into the solution. This observation is consistent with the results from Hedlund *et al.* (2017) who have proposed that coagulation proceeds in two main steps: first, the inflow of water causes solvent desorption and the precipitation of cellulose, thereafter the solvent diffuses out of the solution, as shown in Figure 16.

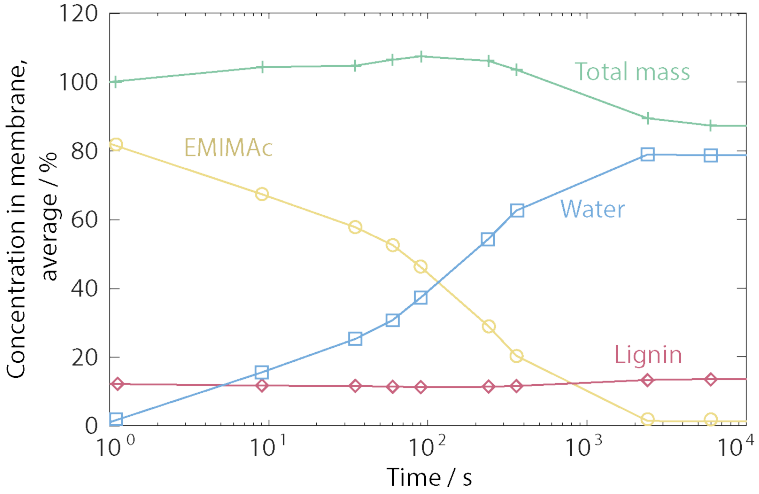

Figure 16. The typical mass flows during coagulation. Note that the time on the x-axis is presented in logarithmic scale.

The diffusivity of EMIMAc was found to be similar for both polymer concentrations, 18 and 27 wt%, as shown in Figure 17. The reason for this may be explained by the assumption that cellulose coagulates into a heterogeneous gel, which was suggested by Hedlund *et al.* (2017), and thus the diffusion of EMIMAc and water take place in the open pores formed by the precipitated cellulose fibrillar network. The diffusivity remainsed unchanged even with 15 wt% EMIMAc, which is realistic considering that 15 wt% is only 2 mol%, *i.e.* much closer to pure water than EMIMAc (Hall *et al.*, 2012). However, when the coagulation bath contained both EMIMAc and acetic acid, the diffusivity of EMIMAc was found to be significantly lower than in the other coagulation baths. A plausible explanation for this is that the diffusion of EMIMAc was hindered by the high concentration of soluble lignin, as shown in Table 3, as dissolved lignin may interact with the EMIMAc and retard mass transport.

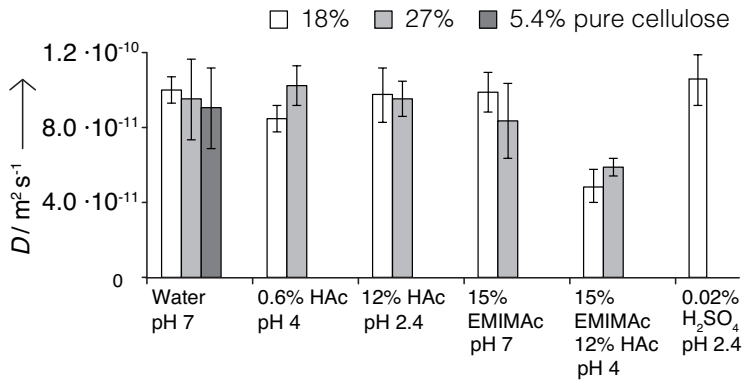

Figure 17. Diffusion coefficients for EMIMAc during coagulation in different coagulation baths for the two solutions with different total polymer concentration.

5.2.1 Leaching of lignin during coagulation

When analyzing the MWD of lignin in spun fibers and comparing it with the initial lignin, it was possible to conclude that low molecular weight lignin had leached out into the coagulation bath, see Figure 18. If a fractionated lignin (RL5 and RL15), was used, the MWD of lignin in fibers was more similar to the added lignin than the unfractionated lignin, indicating less leached lignin.

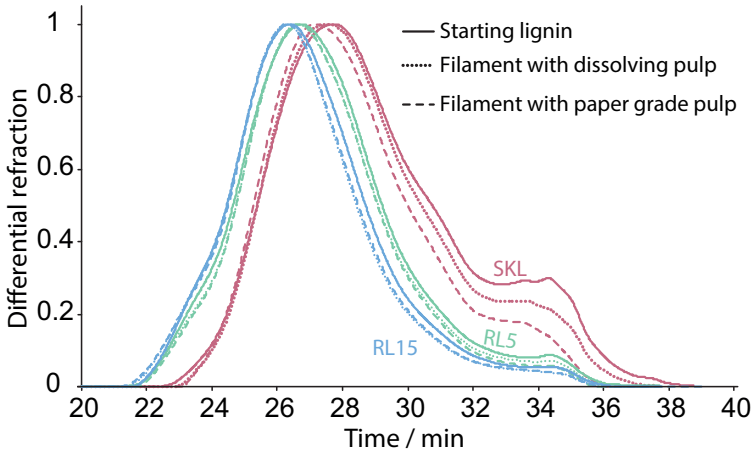

Figure 18. MWD of Softwood Kraft lignin and retentate lignins (RL5 and RL15), and of fibers spun with the same lignin both in combination with dissolving and paper-grade pulp. Small molecules take a longer time to elute than larger molecules.

In addition to that the molecular weight affects the solubility, the literature has previously also reported an enrichment of carboxylic groups in low MW lignin (Bylin *et al.*, 2014), which have a pKa of around 4.4 (Ragnar *et al.*, 2000). The carboxylic groups are, therefore, protonized at a level of pH 4 or lower. Subsequently, in an attempt to reduce leaching of lignin, the level of pH was lowered in the coagulation bath to reduce the solubility of the low MW lignin. An analysis of the lignin content of washing baths showed a decrease in the leaching of lignin at lower pH, as shown in Figure 19. When the coagulated membrane was transferred from the coagulation bath to the washing bath, it carried some liquid and, in most cases, rendered a washing bath with a pH level similar to that of the coagulation bath. A clear trend towards less lignin leached was found when the pH dropped to a level of 4 or below in the washing baths. Consequently, these results indicate the influence of the protonation of carboxylic groups on lignin yield.

However, during the initial stage of coagulation, a low pH level had no benefit for lignin yield, as shown in Figure 20. Instead, it seemed that the pH level had no effect on leached lignin at times below 6000 s. This observation is visible in the black curves in Figure 20 where pH was reduced with sulfuric acid. On the other hand, a fair assumption based on Figure 20 is that equilibrium had not been reached, perhaps with the exception of membranes coagulated at pH 1.3 (sulfuric acid).

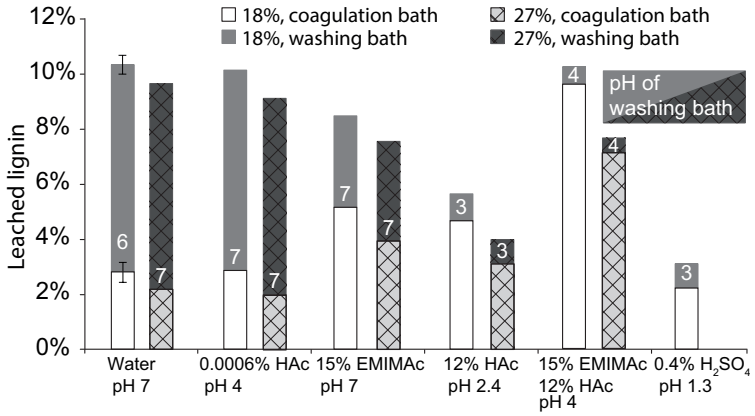

Figure 19. Lignin leached after 6000 s in the coagulation bath (light shaded bars) and in the washing baths (dark shaded bars). White digits inside the washing bath bars indicate the pH levels.

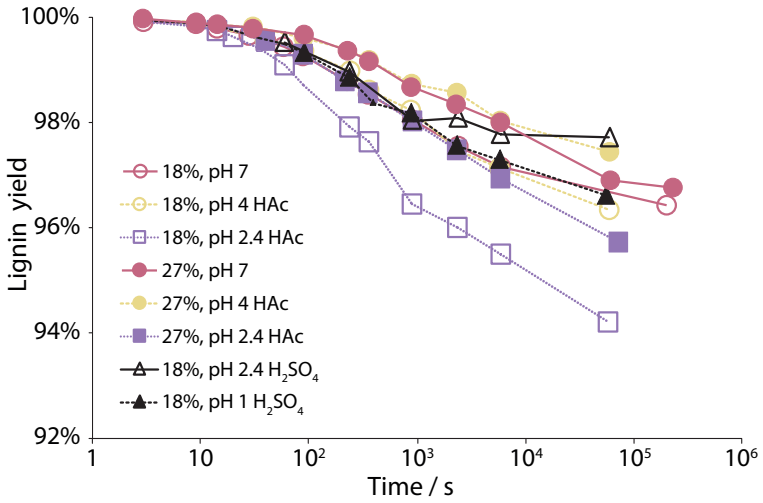

Figure 20. Leaching of lignin as a function of time in coagulation baths with different pH levels.

A comparison of the lignin solubility values in Table 3 and Figure 19 shows that less lignin was dissolved during the coagulation (6000 s) of a lignin-cellulose solution than if a pure lignin-EMIMAc solution was coagulated, indicating that the cellulose network, in one way or another, encloses lignin. In the attempt to further analyze the mechanism of lignin leaching from a lignin-cellulose solution the total polymer concentration (but same lignin:cellulose ratio) was increased. It was found that the same absolute amount of lignin was leached from the solution regardless of its polymer concentration, 18 or 27 wt%, as shown in Figure 21. Consequently, relatively less lignin was leached in the same coagulation liquid for a solution with a 27% polymer concentration. The results are in line with Protz *et al.* (2021b), who have analyzed the lignin content of spun cellulose-lignin fibers. Despite the fact

that the reported lignin losses were substantially higher than what was found in this work, they concluded that if the lignin content of the cellulose-lignin solution was increased, the lignin yield increased as well.

Assuming that cellulose coagulates into a fibrillar network, a plausible explanation would be that the lignin solubility limit is reached in the liquid phase inside the cellulose pores formed during the coagulation, which causes excess lignin to precipitate. Thus, a solution with a higher polymer concentration would lead to the encapsulation of a larger fraction of the lignin and, consequently, a higher lignin yield.

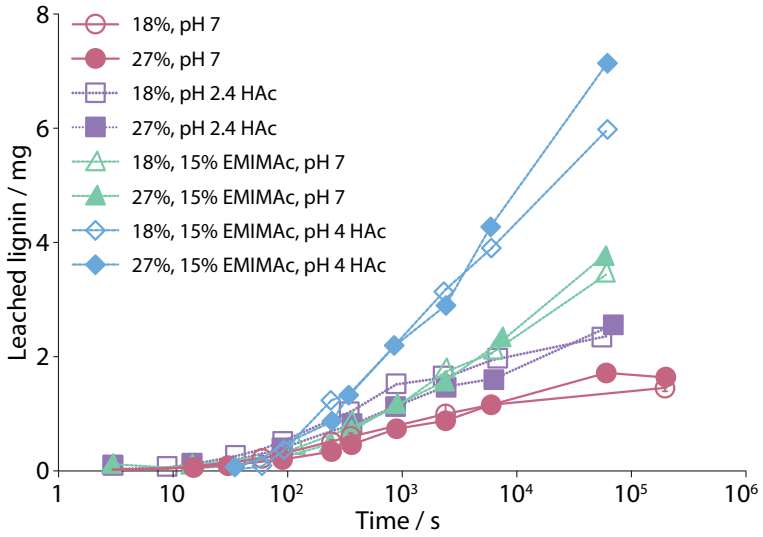

Figure 21. Absolute amounts of lignin leached into the coagulation bath after different amounts of time.

Based on the membrane coagulation results, a coagulated structure was proposed and is illustrated in Figure 22. The figure shows a porous network where lignin has dissolved inside the pores of the cellulose. Leaching of lignin is, thereby, limited by the solubility of lignin within these pores. The most efficient strategies to limit lignin leaching were found to be use of a high molecular weight lignin (*eg.* obtained from membrane fractionation of raw lignin) and/or an acidic washing step.

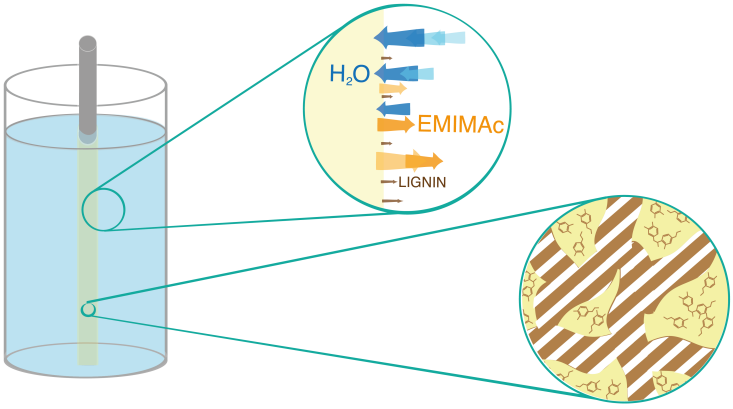

Figure 22. Illustration of the coagulation of a lignin-cellulose membrane. The different mass flows are illustrated in the upper circle, and a proposed structure and plausible mechanism of leaching of lignin are shown in the lower circle.

5.3 Fiber properties

Since lignin and cellulose have such different characteristics, such as molecular weight, morphology, and crystallinity, it is highly relevant to analyze how the structure of the spun fiber is affected by the lignin ratio. The fibers displayed different shades of brown, depending on the lignin content, Figure 23. After observation in SEM, it was clear that air-gap spinning of lignin-cellulose EMIMAc solutions renders circular flexible fibers with smooth surfaces, as illustrated in Figure 24 where a fiber with 70% lignin has been tied into a small knot.

Figure 23. Photography of three cellulose-lignin fibers containing different amounts of lignin. Top: 67, Mid: 33, Bot: 10 wt% lignin.

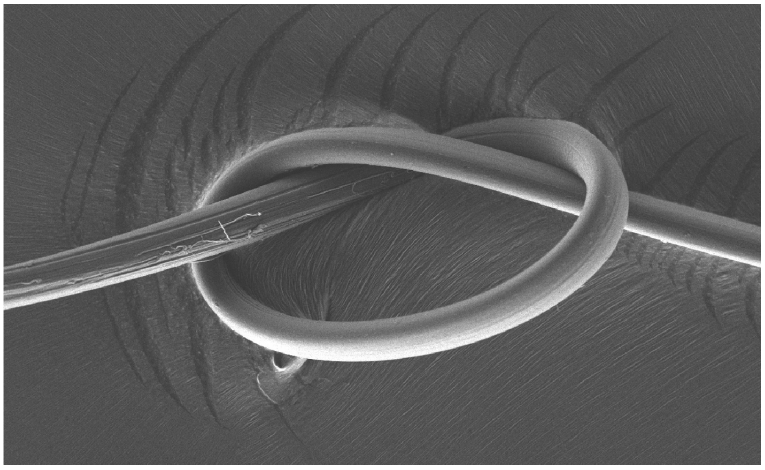

Figure 24. SEM-image of flexible precursor fiber with lignin:paper grade pulp, 70:30.

A fiber with 70% lignin had, as expected, lower tenacity and modulus than pure cellulose fibers, as shown in Table 4, approximately half in both tensile strength and modulus. The impaired mechanical properties are likely due to the lower MW of the lignin: the average MW of the cellulose is approximately 20 times higher than the average MW of lignin (Klemm *et al.*, 1998; Olsson *et al.*, 2017). The mechanical properties may also be affected by the non-linear structure of lignin in comparison with cellulose and thus the possibly changed structure within the fiber with the addition of lignin. This observation is in line with literature data on similar cellulose-lignin fibers (Ma *et al.*, 2015). Otherwise, no significant differences in the mechanical properties of the precursor fibers were found for the different types of lignin, filtered (RL5 and RL15), non-filtered (lignin), or cellulose (paper grade or dissolving pulp). Similar findings have been reported by Trogen *et al.* (2021), who have found that the origin of lignin, beech or spruce, had no significant impact on the tenacity of spun fibers.

The review by Frank *et al.* (2014) states that the precursor must exhibit a preferred molecular orientation to ensure a carbon fiber with high modulus and strength. The draw ratio can be used to improve the tensile strength and modulus of pure cellulose fibers,(Elsayed *et al.*, 2021), however, it is not obvious that this effect remains for fibers with a high lignin content since lignin is a non-linear and amorphous macromolecule. As can be seen in Figure 25, the mechanical properties for a lignin-cellulose fiber did improve with draw ratio. The tenacity of the fibers seems to stagnate after a draw ratio of 8, but the modulus increases over the whole measured range of draw ratios. The mechanic properties are in line with the stress-draw ratio curve in Figure 14 - that the structure in a lignin:cellulose fiber evolves beyond the draw ratio at which point the corresponding cellulose fiber reaches a maximum extendable state. Consequently, it seems motivated to perform spinning at a temperature corresponding to the maximum critical draw ratio to optimize fiber properties.

Table 4. Fibers of different pulp and lignin types. For all fibers that contained lignin (regardless of lignin type) the lignin:cellulose ratio was 70:30. All fibers were spun with a draw ratio of 4 except the pure dissolving pulp solution where a draw ratio of 3.3 was used.

	Diameter		Tenacity		Tensile Modulus	
Raw material	**/ µm**	**±**	**/ MPa**	**±**	**/ GPa**	**±**
Dissolving pulp	21.3	1.0	382	31	15.2	0.8
Paper grade pulp	26.9	2.1	452	28	14.6	1.4
Lignin:Dissolving pulp	24.8	1.2	198	14	8.2	0.5
Lignin:Paper grade pulp	22.1	1.5	183	61	8.9	0.5
RL15:Dissolving pulp	24.0	1.3	189	33	7.7	0.8
RL15:Paper grade pulp	23.8	1.4	182	31	8.3	0.4
RL5:Dissolving pulp	24.4	0.9	191	22	7.5	0.4
RL5:Paper grade pulp	25.1	0.9	154	35	7.9	0.4

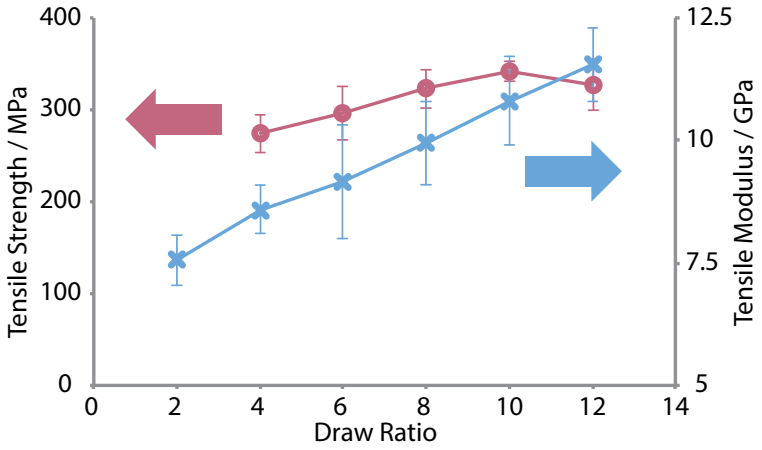

Figure 25. Mechanical properties of lignin:cellulose fibers spun from the L50C8 solution at 60 °C.

To analyze if the lignin had a preferred orientation in the fibers were analyzed with ROSMAS-NMR, **Paper IV**. The technique is chemical sensitive, which means that it is possible to analyze the orientation of each component in a fiber. The cellulose exhibited a preferred orientation, however, no anisotropy was found for the lignin in these fibers.

The birefringence of fibers with a lignin content of 0 - 67% was measured, and the results are summarized in Figure 26. The decrease in birefringence with lignin content is consistent with other studies on lignin/cellulose fibers (Ma *et al.*, 2015; Trogen *et al.*, 2021). Since lignin was found to be isotropic within the fiber, and is thus not expected to contribute to the birefringence, the values were also normalized with respect to cellulose (in this case the pulp ratio added to the spinning solution).

It can be noted that the birefringence of the normalized values is rather constant despite lignin content in fiber, which is in line with the results by Protz *et al.* (2021a), measured with X-ray analysis, indicating a similar orientation of cellulose regardless of lignin content.

Trogen *et al.* (2021) have also normalized birefringence data of lignin-cellulose fibers with respect to cellulose content and found a decrease in the normalized data for fibers with 50% lignin. This finding lead them to the conclusion that high lignin ratios impair cellulose orientation. However, the maximum lignin ratio used in the work of Trogen *et al.* (2021) and Ma *et al.* (2015) was 50% and, if the same lignin ratio would have been the maximum also in this work, the same conclusions would probably have been drawn due to the slight dip in the normalized birefringence for 50% lignin, and the reason for this is not yet known. Further studies, preferably with high spatial resolution, are thus needed to analyze how cellulose fibrillar size and orientation are affected by lignin.

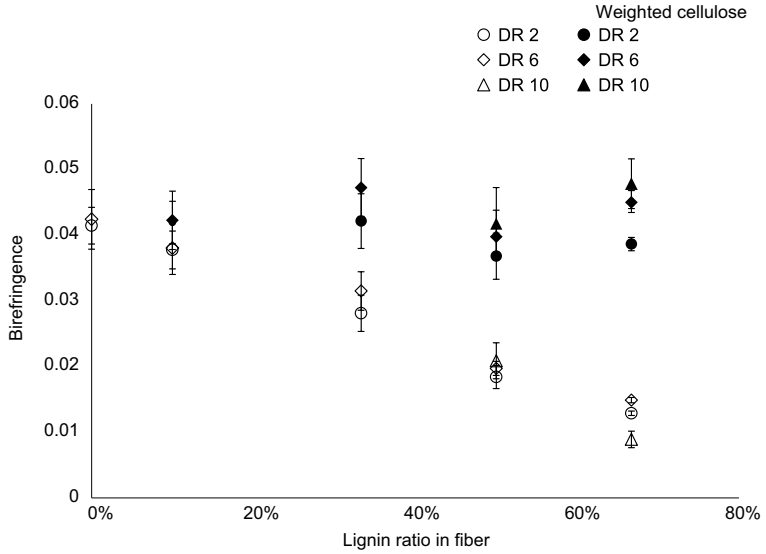

Figure 26. Birefringence of lignin:cellulose fibers

5.4 Carbon fibers made from lignin and cellulose

Lignin-cellulose fibers spun in this work have been converted into carbon fibers, and the results are summarized in Table 5. As was found for the precursor fibers, the choice of pulp, dissolving or paper grade, does not seem to have an impact on the mechanical properties. Notably is that the mechanical properties of the carbon fibers from lignin-containing precursors are almost comparable to the carbon fibers from pure cellulose fibers, the difference is less than when the precursor fibers were compared, cf. Table 4. The carbon fiber yield was also nearly doubled when a lignin-containing precursor was used, and the yield was closer to the theoretical value, see **Papers I**, Figure 7.

Table 5. Properties of carbon fibers produced from different precursor fibers

	Diameter		**Tenacity**		**Tensile Modulus**		
Raw material	**/ µm**	**±**	**/ GPa**	**±**	**/ GPa**	**±**	**Yield**
Dissolving pulp	9.0	1.0	1.00	0.23	74	18	23%
Paper grade pulp	9	1.1	0.92	0.24	71	12	20 %
Lignin:Dissolving pulp	15	0.6	0.88	0.14	65	3.8	40%
Lignin: Paper grade pulp	14	1.2	0.88	0.19	65	5.4	40%

A stabilizion step is often required in the manufacturing of carbon fibers in order to convert the precursor fiber into a thermoset and, thus, prevent fiber fusion during carbonization. However, Bengtsson *et al.* (2019) have shown that stabilization can be omitted for air-gap spun lignin-cellulose fibers, without any fusion of the carbon fibers. On the other hand, skipping the stabilization step was not beneficial to the mechanical properties of the carbon fibers. The strongest lignin cellulose fibers (1.1 GPa TS, 76 GPa TM) were created from thin precursor fibers (14 µm spun with a draw ratio of 7) with a total stabilization time of 2 h, without process optimization (Bengtsson *et al.*, 2019). Thus, the thin carbon fibers were both stronger and stiffer compared to the lignin-cellulose-based carbon fibers in Table 5. The strength of carbon fibers is known to correlate well to their diameter due to the lower probability of defects in a smaller volume (Nordström *et al.*, 2013). In this case, if the increased strength was a result of - or a combination of - the increase in draw ratio or a smaller diameter was not fully elucidated. Additional investigations are needed to understand the effect of process parameters, both in precursor production and the subsequent thermal treatments, on the micro-structure and resulting mechanical properties of precursor and carbon fiber, respectively.

6 Concluding remarks

For several reasons, the great potential of air-gap spun lignin-cellulose fibers as carbon fiber precursors is easily recognized. The use of such abundant, bio-based and carbon-rich raw materials is a very well-suited combination to achieve affordable and sustainable carbon fibers. Furthermore, air-gap spinning enables a high molecular orientation within the fiber, which is a desired property of carbon fibers. In addition, the possibility to use the LignoBoost Kraft lignin macromolecules without any additional post-processing or functionalization is an advantage over many other lignin carbon-fiber attempts. In the present work, the effect of the mixture of lignin-cellulose on the extrusion, coagulation and fiber structure was studied.

For the prepared lignin-cellulose solutions, two main types of break-up mechanisms during air-gap spinning have been identified. The dominant type was dependent on temperature. At lower temperatures, the critical draw ratio was suggested to be limited by the breaking stress of the solution. As the temperature of the spinning solution increased, draw resonance became visible in the video recordings of the breakage. Thus, draw resonance was proposed to be the dominant mechanism at higher temperatures. The existence of two different break-up mechanisms was also confirmed in the take-up force measurements. Consequently, an optimal spinning temperature exists for each solvent composition and for specific spinning parameters, such as choice of die and extrusion velocity.

The addition of lignin increased the maximal critical draw ratio of a cellulose solution in the studied solvent system. The difference in critical draw ratio between solutions with and without lignin was especially clear at higher temperatures of solution. However, this spinning behavior could not be explained by shear rheology or the surface tension of the solutions. When the stress in a solution during spinning at these temperatures was compared, it was found that the maximum stress was substantially greater if the solution contained lignin. A possible explanation for this is that lignin contributes with interactions within the solution that hinder cellulose-cellulose slippage and, in such way, improve spinning stability. The results underline that predicting the spinnability of a solution is a difficult task, and new methods should be consulted or developed for such forecasts.

During the coagulation of a lignin-cellulose solution a minor and low molecular weight fraction of the Kraft lignin leaches out. However, the addition of lignin to a cellulose solution does not seem to impair or retard coagulation as the diffusivity of EMIMAc is similar in both cases. The amount of leached lignin was found to depend on lignin solubility in the coagulation bath and the total polymer concentration in the spinning solution. From the results, a coagulated structure was proposed where leaching of lignin was suggested to be limited by the solubility of lignin within the coagulated cellulose pores, with the mass transport of lignin out of the fiber as the rate determining step.

The hypothesis, how cellulose and lignin may contribute to the properties of the spun fiber, was confirmed as it was found that by combining cellulose and lignin, it was possible to gain advantages from both materials: strength from cellulose and yield from lignin. Cellulose-lignin based carbon fibers showed promising mechanical properties and high carbon yield. Furthermore it could be concluded that the mechanical properties of the precursor fiber were not significantly affected by the choice of choice of pulp or lignin included in this work, fractionated or not. From the mechanical properties of fibers with 50:50 lignin:cellulose spun with different draw ratios, it was possible to conclude that both the strength and, in particular, the modulus of the lignin-cellulose fibers increased with a higher draw ratio. The results show the benefit of a high critical draw ratio and motivates to perform spinning at the temperature of maximum critical draw ratio. The lignin phase in the spun fibers exhibited no preferred orientation, regardless of draw ratio, as determined from ROSMAS NMR measurements, while the cellulose was found to be anisotropic.

Conclusions are that the addition of lignin to cellulose solutions does not hinder the coagulation process nor formation of oriented cellulose within the spun fiber, and it enables higher draw ratios during spinning. If strategies to improve the mechanical properties of the final carbon fiber are successful, then air-gap spun lignin-cellulose fibers are believed to show great potential in becoming commercially available.

7 Future work

There remain several scientific and industrial aspects regarding spinning of lignin-cellulose fibers that are worth investigating. These issues include spinnability, recycling of the solvent, the adhesion of spun fibers, and the strength of the precursor fiber.

The findings on the effect of lignin and spinnability shows that further investigations on predicting spinnability are needed. For example, new types of elongational viscosity measurements that are adapted to the relevant viscosity range could be developed. There are currently CaBER for low-viscosity and filament extensional rheometers for polymer melts, however, there are no available instruments for concentrated polymer solutions. Another option would be to include large amplitude oscillatory shear (LAOS) rheology, where the solutions are analyzed during larger deformations. This would give better correlation with spinning behavior . It would also be interesting to perform spinning with *in-situ* X-ray analysis to evaluate the orientation and existence of any aggregates during spinning. Further interesting analysis would be to perform spinning with *in-situ* X-ray analysis during spinning.

Recycling of the solvent would be necessary to achieve an economically viable process. Ionic liquids are safe and powerful solvents for cellulose and lignin. However, no efficient recycling method exists yet for this type of solvents. Recycling also has to consider the lignin dissolved in the coagulation bath, or lignin leaching should be hindered from the beginning. The stickiness of fibers after spinning also requires more work to find the underlying mechanism causing it, and thereby be able to omit the adhesion during the sequential carbonization.

The strength of the lignin-cellulose-based carbon fibers is currently not high enough to replace commercial carbon fibers. The carbonization step was not optimized for the carbon fibers produced within this work. This step could have substantial effect on the mechanical properties. Furthermore, if looking for strategies to improve the strength of the precursor fibers, evaluating the choice of lignin could be one route. The use of a lignin with a more linear molecular structure may attain a preferred orientation with the fibers (Ragauskas *et al.*, 2014). Furthermore, draw

ratio during spinning may not be the only option in inducing an orientation within the fibers. Since the precursor fibers show a T_g (Bengtsson *et al.*, 2019), potentially the molecular structure in the fibers could be influenced also after coagulation. In melt spinning of fibers, drawing is commonly performed to enhance the mechanical properties, *i.e.* the spun fibers are stretched in warm or cold atmosphere, and such a production step may also be beneficial to lignin-containing fibers.

8 Acknowledgements

This thesis and the work behind it was partly performed within the project LightFibre, a collaboration between RISE, Chalmers, KTH, SCA, and Valmet, and financed by the Swedish Energy Agency, Energimyndigheten. A number of people have greatly contributed with support and inspiration during the work. I would like to acknowledge the following people in particular:

- Hans Theliander, my main supervisor and examiner, for excellent guidance and invaluable feedback.
- Kerstin Jedvert, my advisor, for your encouragement and for asking the right questions when I come to you with new ideas.
- Everyone in the LightFibre project. Especially Andreas Bengtsson, my "PhD twin", its been really fun working with you. This was only the beginning!
- My co-authors Leo Svenningsson and Artur Hedlund, for great discussions, I learned a lot!
- Carina Olsson, my initial advisor. Thank you for giving me the chance to work within this field.
- The Fiber development unit at RISE, such a great environment to be a part of. Special thanks to Tobias Köhnke, you have always shown great interest and provided valuable feedback.
- The other PhD students and employees at SIKT for always making me feel welcome, even throughout the past Corona-year.
  Special thanks to Maria Gunnarsson 💎
- My family, I miss you when I'm not with you,
  and Johan and Wilmer, there are no ordinary weekdays with you.

9 Bibliography

Baker, D. A, & Rials, T. G. 2013. Recent advances in low-cost carbon fiber manufacture from lignin. *Journal of Applied Polymer Science*, **130**(2), 713–728.

Bechert, M, & Scheid, B. 2017. Combined influence of inertia, gravity, and surface tension on the linearstability of Newtonian fiber spinning. *Physical Review Fluids*, **2**, 113905.

Bengtsson, A, Bengtsson, J, Sedin, M, & Sjoholm, E. 2019. Carbon fibers from Lignin-Cellulose Precursors: Effect of stabilization conditions. *ACS Sustainable Chemistry Engineering*, **7**, 8440–8448.

Bylin, S, Wells, T, Sun, Q, Ragauskas, A. J, & Theliander, H. 2014. Lignin structure and aggregation behavior in a two-component ionic liquid solvent system. *BioResources*, **9**, 6002–6018.

Calvo-Flores, F. G, & Dobado, J. A. 2010. Lignin as renewable raw material. *ChemSusChem*, **3**, 1227–1235.

Casas, A, Omar, S, Palomar, J, Oliet, M, Alonso, V. M, & Rodriguez, F. 2013. Relation between differential solubility of cellulose and lignin in ionic liquids and activity coefficients. *RSC Advances*, **3**, 3453–3460.

Clough, M. T, Geyer, K, Hunt, P. A, Son, S, Vagt, U, & Welton, T. 2015. Ionic liquids: not always innocent solvents for cellulose. *Green Chemistry*, **17**, 231.

Collier, J, Petrovan, S, Patil, P, & Collier, B. 2005. Elongational rheology of fiber forming polymers. *Journal of Materials Science*, **40**, 5133–5137.

Cox, W, & Merz, E. 1958. Correlation of dynamic and steady flow viscosities. *Journal of Polymer Science*, **28**(118), 619–622.

Crestini, C, Lange, H, Sette, M, & Argyropoulos, D. 2017. On the structure of softwood kraft lignin. *Green Chemistry*, **19**(17), 4104–4121.

Culebras, M, Beaucamp, A, Wang, Y, Clauss, M. M, Frank, E, & Collins, M. N. 2018. Biobased structurally compatible polymer blends based on lignin and thermoplastic elastomer polyurethane as carbon fiber Precursors. *ACS Sustainable Chemistry Engineering*, **6**, 8816–8825.

Demay, Y, & Agassant, J-F. 2014. An overview of molten polymer drawing instabilities. *International Polymer Processing Journal*, **29**, 128–139.

El Seoud, O, Kostag, M, Jedvert, K, & Malek, N. I. 2020. Cellulose regeneration and chemical recycling: Closing the "Cellulose Gap" using environmentally friendly benign solvents. *Macromolecular Materials and Engineering*, **305**, 1900832.

Elsayed, S, Helminen, J, Hellsten, S, C, Guizani, Witos, J, Rissanen, M, Rantamäki, A. H, Hyväri, P, Varis, P, Wiedmer, S. K, Kilpeläinen, I, & Sixta, H. 2020. Recycling of superbase-based ionic liquid solvents for the production of textile-grade regenerated cellulose fibers in the lyocell process. *ACS Sustainable Chemistry Engineering*, **8**(37), 14217—-14227.

Elsayed, S, Hummel, M, Sawada, D, Guizani, C, Rissanen, M, & Sixta, H. 2021. Superbase-based protic ionic liquids for cellulose filament spinning. *Cellulose*, **28**, 533–547.

FAOSTAT. 2019. Forestry, Production and Trade. *Food and Agriculture Organization of the United Nations*, http://www.fao.org/faostat/en/data/FO.

Fink, H-P, Weigel, P, Purz, H. J, & Ganster, J. 2001. Structure formation of regenerated cellulose materials from NMMO-solutions. *Progress in Polymer Science*, **26**(9), 1473–1524.

Frank, E, Steudle, L. M, Ingildeev, D, Spörl, J. M, & Buchmeiser, M. R. 2014. Carbon fibers: Precursor systems, processing, structure, and properties. *Angewandte Chemie - International Edition*, **53**(21), 5262–5298.

Garoff, N, Protz, R, Erdmann, J, Ganster, J, & Lehmann, A. 2015. Fiber and a process for the manufacture thereof. US10626523B2.

Garoff, N, Protz, R, Erdmann, J, Ganster, J, & Lehmann, A. 2016. Manufacturing of a shaped body. US20180305844A1.

Garoff, N, Protz, R, Erdmann, J, Ganster, J, & Lehmann, A. 2019. A process for the manufacture of a precursor yarn. US20190085484A1.

Gellerstedt, G. 2015. Softwood Kraft Lignin: Raw material for the future. *Industrial Crops and Products*, **77**, 845–854.

Gellerstedt, G, & Henriksson, G. 2008. Lignins: major sources, structure and properties. *Chap. 9, pages 201–224 of:* Belgacem, M, & Gandini, A (eds), *Monomers, Polymers and Composites from Renewable Resources*. Elsevier Science.

Gellerstedt, G, Sjöholm, E, & Brodin, I. 2010. The Wood-Based Biorefinery: A Source of Carbon Fiber? *The Open Agricultural Journal*, **3**, 119–124.

Glasser, W. G, Rials, T. G, Kelley, S. S, & Davé, V. 1996. Studies of the molecular interaction between cellulose and lignin as a model for the hierarchical structure of wood. *Chap. 19, pages 265–282 of: American Chemical Society Symposium series 688*. Orlando, FL: American Chemical Society.

Gries, T, Veit, D, & Wulfhorst, B. 2015. *Textile Technology, An Introduction*. 2 edn. Munich: Carl Hanser Verlag.

Gupta, V. B. 1997. *Solution-spinning processes*. Dordrecht: Springer Netherlands. Pages 124–138.

Hall, C, Le, K. A, Rudaz, C, Radhi, A, Lovell, C. S, Damion, R. A, Budtova, T, & Ries, M. E. 2012. Macroscopic and microscopic study of 1-Ethyl-3-methylimidazolium acetate-water mixtures. *The Journal of Physical Chemistry B*, **8**, 12810–12818.

Hauru, L. K. J, Hummel, M, Michud, A, & Sixta, H. 2014. Dry jet-wet spinning of strong cellulose filaments from ionic liquid solution. *Cellulose*, **21**(6), 4471–4481.

Hauru, L. K. J, Hummel, M, Nieminen, K, Michud, A, & Sixta, H. 2016. Cellulose regeneration and spinnability from ionic liquids. *Soft Matter*, **12**(5), 1487–1495.

Haward, S. J, Sharma, V, Butts, C. P, McKinley, G. H, & Rahatekar, S. S. 2012. Shear and extensional rheology of cellulose/ionic liquid solutions. *Biomacromolecules*, **13**, 16881699.

Hedlund, A, Köhnke, T, & Theliander, H. 2017. Diffusion in ionic liquid-cellulose solutions during coagulation in water: mass transport and coagulation rate measurements. *Macromolecules*, **50**, 8707–8719.

Heinze, T, Petzold-Welcke, K, & van Dam, J. E. G. 2012. *Polysaccharides: Molecular and Supramolecular Structures. Terminology.* Vienna: Springer Vienna. Pages 23–64.

Henriksson, G. 2017. What are the biological functions of lignin and its complexation with carbohydrates? *Nordic Pulp Paper Research Journal*, **32**(4), 527–541.

Hermansson, F, Janssen, M, & Svanström, M. 2019. Prospective study of lignin-based and recycled carbon fibers in composites through meta-analysis of life cycle assessments. *Journal of Cleaner Production*, **223**, 946–956.

Hermanutz, F, Vocht, M. P, Panzier, N, & Buchmeiser, M. R. 2018. Processing of Cellulose Using Ionic Liquids. *Macromolecular Materials and Engineering*, **304**(2), 309–315.

Hummel, M, Michud, A, Asaadi, S, Ma, Y, Hauru, L, Hartikainen, E, & Sixta, H. 2015. Rheological requirements for continuous filament spinning of cellulose-ionic liquid solutions. *Annual transactions of the nordic rheology society*, **23**, 13–20.

Idström, A, Gentile, L, Gubitosi, M, Olsson, C, Stenqvist, B, Lund, M, Bergquist, K-E, Olsson, U, Köhnke, T, & Bialik, E. 2017. On the dissolution of cellulose in tetrabutylammonium acetate/dimethyl sulfoxide: a frustrated solvent. *Cellulose*, **24**, 3645–3657.

Ishihara, H, & Kase, S. 1976. Studies on melt ppinning. VI. Simulation of draw resonance using newtonian and power law viscosities. *Journal of Applied Polymer Science*, **20**, 169–191.

Janesko, B. G. 2011. Modeling interactions between lignocellulose and ionic liquids using DFT-D. *Phys. Chem. Chem. Phys.*, **13**, 11393–11401.

Jin, J, Ding, J, Klett, A, Thies, M. C, & Ogale, A. A. 2018. Carbon fibers derived from fractionated–solvated lignin precursors for enhanced mechanical performance. *ACS Sustainable Chemistry Engineering*, **6**(11), 14135–14142.

Klemm, D, Philipp, B, Heinze, T, Heinze, U, & Wagenknecht, W. 1998. *General Considerations on Structure and Reactivity of Cellulose*. Weinheim, Germany: Wiley-VCH. Chap. 2, pages 9–42.

Klemm, D, Heublein, B, Fink, H-P, & Bohn, A. 2005. Cellulose: Fascinating biopolymer and sustainable raw material. *Angewandte Chemie*, **44**, 3358–3393.

Kosan, B, Michels, C, & Meister, F. 2008. Dissolution and forming of cellulose with ionic liquids. *Cellulose*, **15**, 56–66.

Laun, H. M, & Schuch, H. 1989. Transient Elongational Viscosities and Drawability of Polymer Melts. *The Journal of Chemical Physics*, **33**, 1327.

Le, N-D, Trogen, M, Ma, Y, Varley, R. J, & Hummel, M. 2020. Cellulose-lignin composite fibers as precursors for carbon fibers: Part 2 - The impact of precursor properties on carbon fibers. *Carbohydrate polymers*, **250**, 116918.

Lehmann, A, Ebeling, H, & Fink, H-P. 2012. *Method for the production of lignin-containing precursor fibres and also carbon fibres*.

Liang, X, & Liu, H. 2020. High-efficiency recovery of 1-etyl-3-methylimidazolium acetate for sugarcane bagasse pretreatment with industrialized technology. *Separation and Purification Technology*, **238**, 116437.

Liebert, T. 2010. *Cellulose solvents - remarkable history, bright future*. Washington, DC: American Chemical society. Pages 143–178.

Liu, H. C, Chien, A-T, Newcomb, B. A, Liu, Y, & Kumar, S. 2015. Processing, Structure, and Properties of Lignin- and CNTIncorporated Polyacrylonitrile-Based Carbon Fibers. *ACS Sustainable Chemistry Engineering*, **3**(9), 1943–1954.

Liu, Y, Meyer, A. S, Nie, Y, Zhang, S, & Thomson, K. 2018. Low energy recycling of ionic liquids via freeze crystallization during cellulose spinning. *Green Chemistry*, **20**, 493.

Ma, Y, Asaadi, S, Johansson, L S, Ahvenainen, P, Reza, M, Alekhina, M, Rautkari, L, Michud, A, Hauru, L, Hummel, M, & Sixta, H. 2015. High-strength composite fibers from cellulose-lignin blends regenerated from ionic liquid solution. *ChemSusChem*, **8**(23), 4030–4039.

Macosko, C. 1994. *Rheology: Principles, Measurements and applications*. Weinheim, Germany: Wiley-VCH.

Mainka, H, Täger, O, Körner, E, Hilfert, L, Busse, S, Edelmann, F. T, & Herrmann, A. S. 2015. Lignin, an alternative precursor for sustainable and cost-effective automotive carbon fiber. *Journal of Materials Research and Technology*, **4**(3), 283–296.

Malkin, A, & Isayev, A. 2017. *Viscoelasticity*. 3 edn. Toronto: ChemTec Publishing. Chap. 2, pages 43–126.

Meister, F, & Kosan, B. 2015. A tool box for characterization of pulps and cellulose dopes in Lyocell technology. *Nordic Pulp Paper Research Journal*, **30**, 112–120.

Metzger, T. G. 2014. *Temperature shift factor according to the WLF method*. 4 edn. Hanover: Vincentz Network. Chap. 8.7.1, pages 204–209.

Michud, A, Hummel, M, Haward, S, & Sixta, H. 2015. Monitoring of cellulose depolymerization in 1-ethyl-3-methylimidazolium acetate by shear and elongational rheology. *Carbohydrate Polymers*, **117**, 355–363.

Michud, A, Hummel, M, & Sixta, H. 2016. Influence of process parameters on the structure formation of man-made cellulosic fibers from ionic liquid solution. *Journal of Applied Polymer Science*, **133**(30), 1–9.

Morgan, H. 1964. *Process for spinning wholly aromatic polyamide fibers*.

Morgan, P. 2005a. *History and Early Development of Carbon Fibers*. Boca Raton, FL: CRC Press. Chap. 3, pages 65–120.

Morgan, P. 2005b. *Poperties of Carbon Fibers*. Boca Raton, FL: CRC Press. Chap. 20, pages 791–861.

Mortimer, S. A, & Peguy, A. A. 1996. The influence of air-gap conditions on the structure formation of lyocell fibers. *Journal of Applied Polymer Science*, **60**, 1747–1756.

Navard, P, & Haudin, J. M. 1985. Spinning of a cellulose methylmorpholine Oxide Solution. *Polymer Processing Engineering*, **3**, 291–301.

Navard, P, Wendler, F, Meister, F, Bercea, M, & Budtova, T. 2012. *Preparation and Properties of Cellulose Solutions*. Vienna: Springer Vienna. Pages 91–152.

Norberg, I, Nordström, Y, Drougge, R, Gellerstedt, G, & Sjöholm, E. 2013. A new method for stabilizing softwood kraft lignin fibers for carbon fiber production. *Journal of Applied Polymer Science*, **128**(6), 3824–3830.

Nordström, Y, Norberg, I, Sjöholm, E, & Drougge, R. 2013. A new method for stabilizing softwood kraft lignin fibers for carbon fiber production. *Journal of Applied Polymer Science*, **128**(6), 1274–1279.

Öhman, F, Wallmo, H, & Theliander, H. 2007a. An improved method for washing lignin precipitated from black liquor - the key to a new biofuel. *Filtration*, **7**(4), 309–315.

Öhman, F, Wallmo, H, & Theliander, H. 2007b. Precipitation and filtration of lignin from black liquor of different origin. *Nordic Pulp Paper Research Journal*, **22**(2), 188–193.

Olsson, C, & Westman, G. 2013a. *Direct dissolution of cellulose: Background, means and applications*. IntechOpen. Pages 143–178.

Olsson, C, & Westman, G. 2013b. Wet Spinning of Cellulose from Ionic Liquid Solutions–Viscometry and Mechanical Performance. *Journal of Applied Polymer Scienc*, **127**(6), 4542–4548.

Olsson, C, Sjöholm, E, & Reimann, A. 2017. Carbon fibres from precursors produced by dry-jet wet-spinning of kraft lignin blended with kraft pulps. *Holzforschung*, **71**(4), 275–283.

Östlund, Å, Idström, A, Olsson, C, T, Larsson P., & Nordstierna, L. 2013. Modification of crystallinity and pore size distribution in coagulated cellulose films. *Cellulose*, **20**(4), 1657–1667.

Otani, S, Yoshihiko, F, Igarashi, B, & Sasaki, K. 1964. Method for producing carbonized lignin fiber. US3461082A.

Perez, S Mazeau, K. 2005. *Conformations, Structures, and Morphologies of Celluloses*. Boca Raton: CRC Press. Chap. 2.

Petrie, C, & Denn, M. 1976. Instabilities in polymer processing. *AlChE Journal*, **22**, 209–236.

Petrie, C. J. S. 2006a. Extensional viscosity: A critical discussion. *Journal of Non-Newtonian Fluid Mechanics*, **137**, 15–23.

Petrie, C. J. S. 2006b. One hundred years of extensional flow. *Journal of Non-Newtonian Fluid Mechanics*, **137**, 1–14.

Protz, R, Lehmann, A, Ganster, J, & Fink, H-P. 2021a. Solubility and spinnability of cellulose-lignin blends in aqueous NMMO. *Carbohydrate Polymers*, **251**, 117027.

Protz, R, Lehmann, A, Hohrisch, J, Ganster, J, & Fink, H-P. 2021b. Solubility and spinnability of cellulose-lignin blends in specific ionic liquids. *Carbohydrate Polymer Technologies and Applications*, **2**, 1000041.

Pu, Y, Jiang, N, & Ragauskas, A. J. 2007. Ionic liquid as a green solvent for lignin. *Journal of Wood Cemistry and Technology*, **1**(1), 23–33.

Ragauskas, A. J, Beckham, G. T, Biddy, M. J, Chandra, R, Chen, F, Davis, M. F, Davison, B. H, Dixon, R. A, Gilna, P, Keller, M, Langan, P, Naskar, A. K, Saddler, J N, Tschaplinski, T. J, Tuskan, G. A, & Wyman, C. E. 2014. Lignin valorization: Improving lignin processing in the biorefinery. *Science*, **344**, 1246843.

Ragnar, M, Lindgren, C. T, & Nilvebrant, N. O. 2000. pKa-Values of Guaiacyl and Syringyl phenols related to lignin. *Journal of Wood Chemistry and Technology*, **20**(3), 277–305.

Ralph, J, Lundquist, K, Brunow, G, Lu, F, Kim, H, Schatz, P. F, Marita, J. M, Hatfield, R D., Ralph, S. A, Holst Christensen, J, & Boerjan, W. 2004. Lignins: Natural polymers from oxidative coupling of 4-hydroxyphenyl- propanoids. *Phytochemistry Reviews*, **3**, 29–60.

Rauwendaal, C. 2014. *Polymer Extrusion.* 5 edn. Munich, Germany: Hanser Publishers.

Rosenau, T, Potthast, A, Adorjan, I, Hofinger, A, Sixta, H, Firgo, H, & Kosma, P. 2002. Cellulose solutions in N-methylmorpholine-N-oxide (NMMO) – degradation processes and stabilizers. *Cellulose*, **9**, 283—-291.

Schuermann, J, Huber, T, LeCorre, D, Mortha, G, Sellier, M, Duchemin, B, & Staiger, M. P. 2016. Surface tension of concentrated cellulose solutions in 1-ethyl-3-methylimidazolium acetate. *Cellulose*, **23**(2), 1043–1050.

Sixta, H, Potthast, A, & Krotschek, A. W. 2006. Chemical Pulping Processes. *Chap. 4, page 109 of:* Sixta, H (ed), *Handbook of Pulp.* Weinheim: Wiley-VCH.

Sixta, H, Michud, A, Hauru, L, Asaadi, S, Ma, Y, King, A. W. T, Kilpeläinen, I, & Hummel, M. 2015. Ioncell-F: A High-strength regenerated cellulose fibre. **30**(1), 43–57.

Skogsindustrierna. 2019. Statistik - Produktion och handel med massa. https://www.skogsindustrierna.se/om–skogsindustrin/branschstatistik/massa–produktion–och–handel/.

Souto, F, Calado, V, & Pereira Jr, N. 2018. Lignin-based carbon fiber: a current overview. *Materials Research Express*, **5**(7), 072001.

Spörl, J. M, Beyer, R, Abels, F, Cwik, T, Müller, A, Hermanutz, F, & Buchmeiser, M. R. 2017. Cellulose-derived carbon fibers with improved carbon yield and mechanical properties. *Macromolecular Materials and Engineering*, **302**(10), 1700195.

Stibal, W, Schwarz, R, Kemp, U, Bender, K, Weger, F, & Stein, M. 2005. Fibers, 3. General production technology. *Ullmann's Encyclopedia of Industrial Chemistry.*

StoraEnso. 2020. Stora Enso and Cordenka partner to develop bio-based carbon fibers materials. https://www.storaenso.com/en/newsroom/press–releases/2020/5/stora–enso–and–cordenka–partner–to–develop–bio–based–carbon–fiber–materials.

Sudo, K, & Shimizu, K. 1992. A new carbon fiber from lignin. *Journal of Applied Polymer Science*, **44**(1), 127–134.

The Fiber Year. 2019. *World Survey on Textiles and Nonwovens.*

Theander, O, & Westerlund, E. A. 1986. Studies on dietary fiber. 3. Improved procedures for analysis of dietary fiber. *Journal of Agricultural and Food Chemistry*, **34**(2), 330–336.

Trogen, M, Le, N-D, Sawada, D, Guizani, C, Lourençon, Tainise V, Pitkänen, L, Sixta, H, Shah, R, O'neill, H, Balakshin, M, Byrne, N, & Hummel, M. 2021. Cellulose-lignin composite fibres as precursors for carbon fibres. Part 1 – Manufacturing and properties of precursor fibres. *Carbohydrate Polymers*, **252**, 117133.

Vincent, S, Prado, R, Kuzmina, O, Potter, K, Bhardwaj, J, Wanasekara, N. D, Harniman, R. L, Koutsomitopoulou, A, Eichhorn, S. J, Welton, T, & Rahatekar, S. S. 2018. Regenerated cellulose and willow lignin blends as potential renewable precursors for carbon fibers. *ACS sustainable Chemistry & Engineering*, **5**(6), 151–161.

Wang, Y-Y, Meng, X, Pu, Y, & Ragauskas, A. J. 2020. Recent advances in the application of functionalized lignin in value-added polymeric materials. *Polymers*, **12**, 2277.

White, J. L, & Hancook, T. A. 1981. Fundamental analysis of the dynamics, mass transfer, and coagulation in wet spinning of fibers. *Journal of Applied Polymer Science*, **26**, 3157–3170.

White, P. 2001. *Lyocell: The production process and market develoment.* Cornwall, England: Woodhead Publishing. Chap. 4, pages 62–87.

Wirth, B, Warnecke, M, Schmenk, B, Seide, G, & Gries, T. 2011. Filament breaches during air-gap spinning. *Chemical Fibers International*, **61**(1), 64–65.

Woodings, C. 2001. *A brief history of regenerated cellulosic fibres.* Cornwall, England: Woodhead Publishing. Chap. 1, pages 1–21.

Zhang, Y, He, H, Dong, K, Fan, M, & Zhang, S. 2017. A DFT study on lignin dissolution in imidazolium-based ionic liquids. *RSC Adv.*, **7**, 12670–12681.

Ziabicki, A. 1976. *Fundamentals of fibre formation, p. 64.* Bath, Great Britain: Wiley.

Ziabicki, A, & Takserman-Krozer, R. 1964. Mechanism of breakage of liquid threads. *Zeitschrift und Zeitschrift fur Polymers*, **198**, 60–65.